A Bayesian approach to~~New approaches to~~ integrating radiometric dating and varve measurements in intermittently varved sediment~~, Columbine lake, Colorado, USA~~

Stephanie H. Arcusa[1], Nicholas P. McKay[1], Charlotte Wiman[2], Sela Patterson[1], Samuel E. Munoz[2,3], Marco A. Aquino-López[4]

[1]School of Earth and Sustainability, Northern Arizona University, Flagstaff, 86011, USA
[2]Department of Marine and Environmental Sciences, Northeastern University, Marine Science Center, Nahant, 01908, USA
[3]Department of Civil and Environmental Engineering, Northeastern University, Boston, 02115, USA
[4]Centro de Investigación en Matemáticas (CIMAT), Jalisco s/n, Valenciana, 36023 Guanajuato, Gto, Mexico

Correspondence to: Stephanie H. Arcusa (sha59@nau.edu)

Abstract. Annually laminated lake ~~lake~~ sediment can track paleoenvironmental change at high-resolution where alternative archives are often not available. However, information about the ~~both paleoenvironmental change and~~ chronology ~~are~~is often affected by indistinct and intermittent ~~varves~~laminations. Traditional chronology building struggles with these kinds of laminations; typically~~,~~ failing to adequately estimate uncertainty, or discarding the information recorded in the laminations~~s the archive~~ entirely, despite their potential to improve~~annually laminated sediment being a superior archive~~ chronologies. We present an approach that overcomes the challenge of indistinct or intermediate laminations ~~these~~ and other obstacles by using a quantitative ~~varve~~ lamination quality index combined with a multi-core, multi-observer Bayesian ~~varve~~ lamination sedimentation model that quantifies realistic under- and over-counting uncertainties while integrating information from radiometric measurements (^{210}Pb, ^{137}Cs, and ^{14}C) into the chronology. We demonstrate this approach on ~~thin sections~~sediment of indistinct and intermittently ~~varved~~ laminated sequences from alpine Columbine Lake, Colorado. The integrated model indicates 3137 (95% ~~percentile~~ highest density probability range: 2753-3375) varve years with a cumulative posterior distribution of counting uncertainties of -13/+7 % indicative of systematic observer undercounting. ~~The sedimentary features of the thin and complex varves shift through time, from normally graded couplets to couplets interrupted with coarser sub-laminae, to inversely graded couplets. We interpret the normal grading couplets as spring nival discharge followed by winter settling, the coarser sub-laminae as high rainfall events, and the inverse grading as hyperpycnal flows and/or pulses of dust related to human impact changing the varve formation mechanism.~~ O~~O~~ur novel approach provides a realistic constraint on sedimentation rates and quantifies uncertainty in varve counts by quantifying over- and under-counting uncertainties related to observer bias and the quality and variability of the sediment appearance. The approach permits the construction of a ~~varve~~ chronology and sedimentation rates for sites with intermittent or indistinct ~~varves~~laminations, which are likely more prevalent than sequences with distinct ~~varves~~laminations, especially when considering non-lacustrine sequences, and thus, expands the possibilities of reconstructing past environmental change with high resolution.

1 Introduction

The establishment of a reliable chronology for lake sediment is a pre-requisite of paleoenvironmental investigation. As many studies have pointed out, low age uncertainty is necessary to compare events through across space, time, and archive type (e.g., Zimmerman and Wahl, 2020). To that end, annually laminated sediment (i.e., varves) not only presents a unique opportunity to reconstruct variability on a seasonal to annual scale, itbut it also allows for the quantification of sediment accumulation rates on shorter timescales than sequences dated by radiometric techniques (Boers et al., 2017). Sedimentation rates are useful for a wide range of investigations, but especially so for the accurate calculation of fluxes (g cm^2 yr^{-1}) of sedimentary constituents. For paleoenvironmental reconstructions, flux is can be typically a more meaningful measure than alongside abundance or and concentration because it considers changes in the sediment due to time and density. For example, investigations using lake sediment of past aerosol deposition such as dust report different conclusions when flux is used compared to abundance (Arcusa et al., 2019; Routson et al., 2016, 2019). The importance of constraining age and sedimentation rate uncertainty is increasingly recognized and the tools to handle this uncertainty are constantly improving (Aquino-López et al., 2018; McKay et al., 2020θ1).

Despite general improvements, the quantification of uncertainty in varved sediments remains focused on counting. Although there is no standard method for calculating uncertainties in varve chronologies, most are associated with ±1-4 % counting uncertainty with some indistinctly varved sequences having counting errors up to ±15 % (Ojala et al., 2012). Counting errors are often quantified as the root mean squared error of counts from multiple observers along defined transects on multiple cross-dated cores from the same site either as maximum and minimum deviations from the mean or as replicated counts between marker layers (Lamoureux, 2001). Reported error estimates commonly do not include all known error sources.

Error sources are associated with (1) intraer siteinter-core differences in varve counts (missing varves), (2) subjectivity in identifying varves due to varve quality, (3) expert judgement in identifying marker layers, (4) compound single varves that are mis-interpreted as representing multiple years (over counting), (5) indistinct varves that are combined with adjacent varves (under counting), (6) intermittent (floating) varves, (7) technical issues (missing varves), and (8) counting strategies (Fortin et al., 2019; Ojala et al., 2012; Żarczyński et al., 2018; Zolitschka et al., 2015). Although these various sources are often considered individually, they are less frequently considered in concert and rarely considered when estimating sedimentation rates. The variety of error sources makes their quantification an important challenge, especially for sequences with indistinct or intermittent varves.

Sedimentary sequences with indistinct or intermittent varves cannot be used to develop a chronology with conventional techniques as portions ofthe massive sediment or indistinct laminations result in information loss. Yet, such sequences still provide more chronology information than massive sequences and such sequences are likely more prevalent than sequences with perfect varves, especially when considering non-lacustrine settings. The problem is often addressed by subjectively

applying the sedimentation rate estimated from neighboring varved sections, although more mechanistic methods have also been developed. For example, Schlolaut et al. (2012) describe a procedure that analyses the seasonal layer distributions to estimate the number of years of sediment accumulation represented. Although promising, such a method of varve interpolation has yet to be integrated with a complete accounting of all other errors.

Few previous works have attempted to assess varve counting errors ~~associated with varve counts by their sources~~based on the cause of the errors. For example, Fortin et al. (2019) developed a Bayesian probabilistic model to incorporate three sources of uncertainty related to the subjectivity in identifying varves, ~~inter-site~~~~intra-site~~inter-core differences, and a combination of the likelihood of over- and under-counting by the observer and the proper identification of isochronous marker layers. Although ~~this~~ their model provided a clearer picture of the sources of uncertainty, it did not go as far as addressing the problem of indistinct varves ~~(~~such as those deposited during the 20th century as glacier influence waned~~)~~ nor quantifying the impact of varve quality on the chronology.

Formatted: Superscript

Additionally, errors can be systematic in that the net outcome is ~~one~~ either ~~of~~ over- or under-counting. These systematic biases are typically assessed by comparing the varve chronology to radiometric methods (^{137}Cs, ^{210}Pb, and ^{14}C) and can sometimes be corrected. For example, the agreement between varve and radiometric chronologies can be evaluated objectively through OxCal's V_sequence~~, for example~~ (Bronk Ramsey, 1995; Tian et al., 2005; Zander et al., 2019). The ^{14}C ages can reveal ~~missing sediment~~ intervals where missing ~~varves~~ laminations can be inserted (Tian et al., 2005). However, the process has two major drawbacks. First, the ^{14}C ages could be too old, or, if they are correct, the location of the nonconformity in the sedimentary sequence might be misplaced. Second, this approach does not constrain the uncertainty introduced into the estimation of the sedimentation rate. An improvement could be to create a new chronology that combines information from both the varve profile and the radiometric methods.

Laminated sediment, even when indistinct or intermittent, provides valuable information that should be used to improve chronologies and would provide new opportunities to create records in regions currently lacking (Ramisch et al., 2020). Here, we ~~Using an indistinctly and intermittently laminated sequence from Columbine Lake, Colorado, we Here, we~~ present an approach to quantify age and sedimentation rate uncertainty from such a sequence from Columbine Lake, Colorado, using multiple cores and observers ~~as demonstrated in a case study of an indistinctly and intermittently varved sequence from Columbine Lake, Colorado~~. We expand on the Fortin et al. (2019) Bayesian model to include uncertainty from multiple observers, varve interpolation, and varve quality. We then use Bayesian learning to update prior estimates of the counting uncertainties given the constraints from independent radiometric ages. The result forms the basis for an approach to the development of an annual chronology when laminations are indistinct or intermittent that could be applicable to various types of archives beyond lake sediment. ~~Partly because continuous chronologies are rare, no late Holocene varve sequence has been published from the southern Rocky Mountains up to now. Moreover, the nearest published varved lake record is 250 km away~~

~~(Anderson et al., 2010). The chronology developed here provides the foundation for future high-resolution paleoenvironmental research at Columbine Lake.~~

2 Study Site

Columbine Lake (37.8622º N, 107.7717º W, elevation 3874 m a.s.l.) is a deep, mildly acidic (pH 5), oligotrophic lake in San Juan County, Colorado (Fig. 1). The lake bathymetry is marked by deep pockets, with a maximum depth of ~~27~~ 24 m. Deep and small sub-basins were suspected to favor seasonal stratification and anoxic conditions necessary for varve formation and preservation (Zolitschka et al., 2015). The lake is fed by a small pond and stream to the northwest and drained by Mill Creek to the northeast. The inflow and its resulting delta may have moved over time, as evidenced from satellite imagery. The catchment bedrock is andesite emplaced during the late and middle Tertiary (Lipman and Mcintosh, 2011), and less than 5 % of the area was vegetated in 2017 (Arcusa et al., 2019). The catchment is currently unglaciated and shows no evidence for rock glaciers. The closest documented evidence of a Little Ice Age moraine is near Trinity Peaks (Carrara, 2011). There are no access roads, but historic mining activity is evident at lower elevations and the lake outflow is raised by a 2-m-high earthen dam.

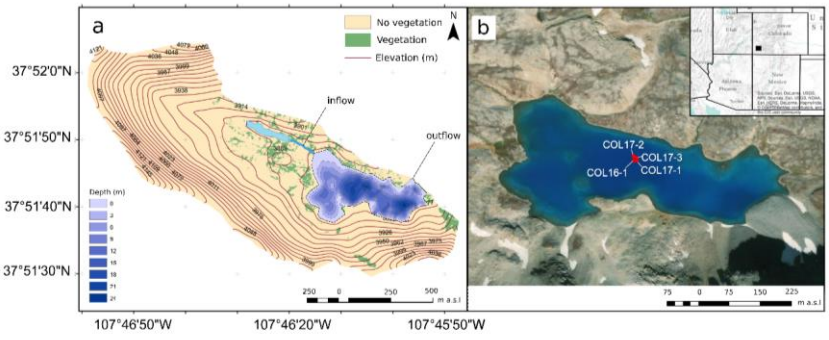

Figure 1. Columbine Lake and its catchment showing (a) bathymetry and (b) coring location (red circles) in southwest Colorado (black rectangle in inset map). Vegetation extent for the year 2017 based on Arcusa et al. (2019). Image credit: Esri, DigitalGlobe, GeoEye, Earthstar Geographics, CNES/Airbus DS, USDA, USGS, AeroGRID, IGN, and the GIS User Community.

~~The climate of Silverton, Colorado (elevation 2865 m) near the study site is typified by a biseasonal climate. Over 80 % of precipitation falls predominantly as snow from October to March (average 560 mm/month total snowfall) from Pacific frontal~~

~~storms, and summer rainfall is associated with the northern extent of the North American Monsoon (Jul-Sep, average 70 mm/month). Average winter (DJF) and summer (JJA) temperature ranges are −18.8 to 2.5 °C and −0.1 to 22.8 °C, respectively (Western Regional Climate Center, 2018). Like much of the Southwest United States, the El Niño Southern Oscillation (ENSO) teleconnection usually results in wet winters during El Niño and dry winters during La Niña (Sheppard et al., 2002).~~

3 Methods

3.1 Coring, description, and correlation

Four sediment cores were collected from Columbine Lake at water depths ranging from ~~25~~ 21 to ~~27~~ 24 m. One 81-cm-long core was taken in August 2016 (COL16-1 collected at 22 m depth) using an aquatic corer, and three 125- to 142-cm-long cores were collected in September 2017 (COL17-1, COL17-2, and COL17-3 collected at respective depths of 23, 24, and 24 m) using a modified UWITEC~~H~~ percussion coring system. All three 2017 cores captured the undisturbed sediment-water interface, but the 2016 core did not. Cores were split, described, and stored at the Sedimentary Records of Environmental Change Lab at Northern Arizona University. Consistent core stratigraphy and marker layers found in all cores except COL17-1 facilitated visual core cross-correlation (**~~Error! Reference source not found.~~** Fig. A1). Core COL17-1 is not laminated, possibly because it was collected ~~at shallower depth~~on the slope of one of the deep ~~, and~~pockets and was not considered further in this study.

~~3.2 Non-destructive core analysis~~

~~To support the visual correlations, cores COL16-1, COL17-2, and COL17-3 were analyzed for non-destructive methods. First, magnetic susceptibility (MS) was measured at 1-cm increment (2-cm measurement diameter resolution) using a Bartington MS2 surface sensor. Then, X-Ray Fluorescence (XRF) was measured at 0.5 and 1 cm intervals (1 cm measurement diameter resolution) at 10, 30, and 50 kV using an Avaatech core scanner at Texas A&M University, College Station. Finally, hyperspectral imaging in the visible to near-infrared range was measured at ~68 µm/pixel using a Specim Ltd. core scanner equipped with a PFE-xx-V10E camera at Northern Arizona University following the method by Butz et al. (2016). The hyperspectral data were used to calculate indices shown to be related to chlorophyll and its degradation products (RABD660) (Trachsel et al., 2010; Yackulic, 2017) as well as chlorite (minimum peak) (Rein and Sirocko, 2002).~~

~~3.3 Destructive core analysis~~

~~To support the sedimentological facies interpretation, various destructive analytical analyses were performed on core COL17-3. Loss-on-ignition and wet and dry bulk density following Dean (1974) used 1-2 cm^3 of sediment weighed wet and dry after freeze-drying for 12 hours, then weighed after burning at 550 ºC for 5 hours in the furnace. An aliquot of 80 mg of material was then used for quantifying the abundance of biogenic silica following an adapted procedure of Mortlock and Froelich (1989). Briefly, the samples were pre-treated to remove organics. Biogenic silica was brought to a solution and measured by~~

~~spectrophotometry. Finally, an aliquot of 200 mg of material was used for grain size analysis. The initial procedure was the same, but the solution of biogenic silica was discarded. Then, sodium hexametaphosphate was added as a dispersant and shaken for 3 hours. Grain size distributions in the 0.04–2000 µm range with 116 classes were analyzed using a laser diffraction Coulter LS13-320 and each sample was measured 5 times.~~

3.~~4~~ 2 Geochronology

This study added three radiocarbon dates to the three previously published by Arcusa et al. (2019) on cores COL17-3 and COL16-1. Macrofossil of terrestrial plants and aquatic insects were pre-treated using standard acid–base–acid procedures and analyzed for radiocarbon activity on Northern Arizona University's MICADAS equipped with the Gas Interface System while it was located at the manufacture's (IonPlus) office in Zurich, Switzerland. Three dates were previously reported by Arcusa et al. (2019) (UCI 196901, UCI 190157, and UCI 188317) for a mixture of small insects and plant fragments. In addition to radiocarbon, Arcusa et al. (2019) also measured ^{210}Pb and ^{137}Cs activities respectively on 20 and 16 dried and homogenized samples over the top 12.5 cm of core COL17-3 using a Canberra Broad Energy Germanium Detector (BEGe; model no. BE3830 P-DET) at the Marine Science Center at Northeastern University.

The radiometric age-depth model was constructed from the concurrent use of Bayesian modeling R (v4.0.2) software packages Bacon (v2.2) (Blaauw and Christen, 2011) and Plum (v0.1.5.1) (Aquino-López et al., 2018). Briefly, Plum is based on a statistical framework, ~~which uses statistical inference to~~ providinge more robust and realistic uncertainties when compared to other lead models such as the Constant Rate of Supply (CRS) method (Appleby and Oldfield, 1978). The concurrent use of Bacon and Plum reduces the artificial break in sedimentation rates at the intersection of the ^{210}Pb and ^{14}C ages, and Plum provides a more natural merger of these techniques as it does not require the pre-modeling of the ^{210}Pb dates. Additionally, we compare Plum to conventional calculations of CRS (Appleby, 2001) and the Constant Flux Constant Sedimentation (CFCS) method (Krishnaswamy et al., 1971) implemented with the R package SERAC (v0.1.0) (Bruel and Sabatier, 2020).

3.~~5~~ 3 Thin sections, sediment imaging, and point measurements

To facilitate investigation, measurement, and ~~counting~~ delineation of the fine laminations, the sediment was subsampled and impregnated with low viscosity epoxy resin following a modified approach of Lamoureux (1994). The percentage of epoxy to acetone was increased multiple times before fully embedding the sediment. Overlapping sediment slabs (7.0 x 3.0 x 1.5 cm) were sampled and placed in an acetone bath for fluid replacement. Acetone was exchanged every 12 hours for five days until no water was left in the sediment. Following fluid displacement, Spurr's Low Viscosity Embedding Resin was exchanged every 12 hours for three days and left to cure for one day at room temperature followed by one day at 40 ºC, one day at 50 ºC, and one day at 60 ºC. Slabs were cut at the Northern Arizona University machine shop and sections were sent to Quality Thin Sections in Tucson, AZ, for mounting and polishing. Images of the thin sections were taken at 2x and 10x magnification under polarized light with a ~~calibrated~~ petrographic polarizing microscope (Carl Zeiss Axiophot) connected to a digital camera (Carl

Zeiss Axiocam) and automated stepping stage (PETROG System, Conwy Valley Systems Ltd (CVS), UK). Individual images were stitched into a mosaic using the Stitching plugin (Preibisch et al., 2009) in ImageJ.

~~To categorize and interpret varve facies, microscopic analyses of elemental composition and grainsize are sometimes used (Cuven et al., 2010; Żarczyński et al., 2019a). In this study, the varves were thinner than the sampling resolution of either destructive (BSi and grain size) or non-destructive (XRF, hyperspectral, and MS) procedures available. Therefore, we used point counts and length measurements directly on individual grains in the slides. At least 100 grains were measured from the varve transects.~~

~~3.6 Statistical analyses~~

~~To support the interpretation of the sedimentary facies, statistical analyses were performed on the results from both destructive and non-destructive procedures. First, the values were binned to match the sampling resolution of the dataset with the lowest resolution using the function bin2d in the R package geoChronR (McKay et al., 2021). Second, the values were standardized to a mean of zero and variance of one standard deviation. Then to identify distinct stratigraphic units, hierarchical cluster analysis was applied using the function chclust R package rioja (Juggins, 2020). To associate units to the variables explaining the most variance, a principal component analysis that was applied with the function PCA in the R package FactoMineR (Lê et al., 2008). Finally, to explore the relationship between variables, correlation analysis was performed using Spearman's rank as the data distribution failed the Shapiro-Wilks normality test in most cases ($p < 0.05$).~~

3.7~~4~~ 64 Probabilistic ~~V~~varve chronology

As with all varve studies, we make an important distinction between laminations and varves. This is especially relevant in this study as a significant portion of the laminations in Columbine Lake sediment are ~~indistinct, and~~indistinct and would not meet the typical definition of a varve couplet. The goal of this study, however, is to characterize the probability of the temporal duration of each lamination~~,~~ and of the sequence as a whole. To make this distinction clear, we use the term "lamination" to refer to what was observed and delineated in the sediments, and the term "varve" to refer to an ~~annually deposited~~annually deposited lamination modeled or simulated in our algorithms. Furthermore, the method does not "count" varves in the traditional sense of the word, it uses delineations of laminations which a model then simulates as a "count". To quantify uncertainty, and ultimate estimate prior probabilities, ~~all of~~all our algorithms are run in ensemble. This means that any given observed lamination may be simulated as a varve in some ensembles and not in others. In section ~~X.Y~~4.6, we argue ~~that as a whole, the~~that the Columbine Lake sequence meets the criteria of a varved sequence, whereas the probability of any given lamination being annual is always < 1.

~~3.7.1 Description of the original varve model~~algorithm

Formatted: Not Highlight

Formatted: Normal

Formatted: Normal

The data analysis in this study expands on ~~the ana~~ codebase in ~~original~~ R (R Core Team, 2019) called ~~"package~~ varveR" (v0.1.0) (McKay, 2019) that builds varve chronologies while quantifying uncertainty due to ~~as it relates to varve~~lamination identification, ~~inter site~~intraer-~~site~~core differences, and likelihoods of over- and under-counting. varveR is a Bayesian probabilistic ~~model~~ algorithm that quantifies age uncertainty by integrating information from the age distribution of marker layers from multiple cores (Fortin et al., 2019). The algorithm ~~model~~ follows two concepts. First, it uses the sedimentological understanding of the likelihood of the correct delineation of the ~~varve~~laminations such as those related to the ease of distinguishing them. Second, it takes advantage of the replication from the marker layers correlating between cores to quantify the likelihood of under- and over-counting and the uncertainty in the total count as a function of depth.

The algorithm~~model~~'s inputs include (1) thicknesses for each ~~varve~~ lamination for each core, (2) site-specific marker layers to stitch the ~~thin~~ sections together into a ~~varved~~ sequence, (3) prior estimates of over- and under-counting and (4~~3~~) ~~intra~~er-~~site~~inter-core marker layers and their prior probabilities. All three inputs are necessary for the code to work. In this study, thickness delineations were created as ArcGIS ArcMap shapefiles (Appendix A Fig. A2). We chose this software for convenience, but in the code's next version we will add the possibility to use open-source shapefiles. ~~Site~~Core-specific marker layers were identified in the overlap between two adjacent thin sections. ~~Inter-site~~~~Intra-site~~Inter-core marker layers were identified in each core using thin sections and core images~~for cross-correlation~~. Lamination boundaries, core-specific and inter-core marker layers ~~All three~~ were identified independently by three observers working ~~independently~~separately, allowing for better quantification for these aspects of uncertainty. All observers ~~to explore uncertainties associated with expert judgment.~~were trained to identify lamination structures and to use common protocols to demarcate lamination boundaries, lamination codes, and marker layers in ArcGIS. Prior to this project the observers had minimal ~~prior~~ experience identifying varves.

The algorithm ~~model~~ uses prior likelihoods of over- and under-counting and updates them, if necessary, as it iterates. The prior likelihoods are selected by the operator but may be the difference in the number of ~~varve~~laminations ~~counted~~ delineated by two observers expressed as a percentage and converted into a probability, ~~for example~~ (e.g., Fortin et al., 2019). With each iteration, the only constraint is that the duration across cores between marker layers must be the same. varveR outputs an *n*-member ensemble of varve counts and thicknesses for each core and a composite of all cores, where *n* is a user-defined number of iterations. The ensemble is used to quantify the uncertainty in depth as a function of varve year and can be transposed to estimate uncertainty in varve year as a function of depth. The algorithm ~~model~~ is completely independent from radiometric age control.

Here,

~~3.7.2 Modifications to the original algorithmmodel: varve quality index and varve emulator~~

Formatted: Font: Italic

Formatted: Font: Italic

~~We expanded the varveR algorithm model to~~we expand on this algorithm to include information on lamination~~varve~~ quality as an indicator of the likelihood of over- and under-counting. Although varve quality indices have been used in past research as a qualitative aide to interpretation (Bonk et al., 2015; Dräger et al., 2017; Żarczyński et al., 2018), here we integrate this information quantitatively. Each ~~varve~~lamination was associated with a code (1, 2, or 3) (Appendix A Fig. A2) with a corresponding distribution of over and under-counting prior probability estimate (Sect. 3.~~7.3~~5). The codes are assigned by the clarity of the ~~varve's~~ lamination's appearance, with a code value of 1 being of higher clarity than a code value of 3. A code of 4 was used when it was difficult to distinguish whether two couplets represented one year with sub laminae, or two separate years. In this case, they were ~~counted~~ delineated as two ~~varve~~laminations, and denoted with a code of 4, which were assigned a 50 % probability of over-counting.

Distinctly laminated sediments interspersed with indistinctly laminated sections comprised zones up to 2 cm thick with weak to absent laminations (Appendix A Fig. A2). These indistinct sections were relatively common, comprising 8.7-19.6 % of the total sediment thickness across observers. For these sections, a code of 5 was assigned. In addition, sections with sediment missing from what could be deemed as technical reasons (e.g., between two adjacent thin sections without overlap or in gaps created by breakage during the embedding process) were assigned a code of 6. Previous studies have addressed the issue of indistinct sections or missing laminae by either interpolating sedimentation rates from nearby varved segments (e.g., Hughen et al., 2004), or using the probability distribution of the varves' seasonal layers to derive sedimentation rates (Schlolaut et al., 2012). These approaches did not work for us, because our Bayesian modelling approach requires an estimate of varve thicknesses for each year rather than an estimate of mean sedimentation rate or missing time. Therefore, to simulate varves in indistinct intervals (or missing), we developed an emulator that randomly chooses a distinctly laminated section of the core and with a length of that section matches the thickness of the interval as nearly as possible. Because laminations at Columbine Lake are very thin (typically < 0.5 mm) relative to the thickness of the indistinct intervals (typically ~ 4 mm), this procedure alone matches the cumulative depth closely. Subsequently, a minute thickness adjustment is applied across the sequence to ensure a perfect match in total thickness and conservation of the depth of the core. This approach is reasonable where other laminated intervals can serve as surrogates for indistinct sections. We argue this is the case for Columbine Lake, as the distribution of the lamination thickness is similar in both cores throughout the sections with distinct laminations (Appendix A Fig. A3). Furthermore, there is no evidence for systematic changes in the mode of deposition in these sections, as the indistinct sections occur throughout both cores, but not always in the same intervals, and the sedimentary features were mostly the same above and below the indistinct sections, suggesting that the indistinct laminations are due to changes in preservation, not the sedimentation process. ~~The application of code 5 is described below. Finally, sections where sediment is likely missing for technical reasons (e.g., between two adjacent thin sections without overlap or in gaps created during the embedding process), were assigned a code of 6, and varves were similarly emulated although the number of missing years is unknown.~~

~~Distinctly varved laminated sediments are interspersed with indistinctly laminated varved sections, which comprise zones up to 2 cm thick with weak to absent ly defined to no visible laminations (Appendix A Fig. A2). These indistinct sections were relatively common, comprising 8.7-19.6 % of the total sediment thickness across observers. For these sections, a code of 5 was assigned. Previous studies have addressed the issue of indistinct varve sections by either interpolating sedimentation rates from nearby varved segments (e.g. Hughen et al., 2004), or using the probability distribution of the varves' seasonal layers to derive sedimentation rates (Schlolaut et al., 2012). Because oOur varveR approach requires an estimate of varve thicknesses for each year rather than an estimate of mean sedimentation rate or missing time, these solutions are insufficient. Instead, we simulate varves through these sections.~~

~~To simulate varves in indistinct intervals, we developed an varve emulator that randomly chooses a distinctly varved laminated section of the core and with a length of that section matches the thickness of the interval as nearly as possible. Because laminations at Columbine Lake are very thin (typically < 0.5 mm) relative to the thickness of the indistinct intervals (typically ~ 4 mm), this procedure alone matches the cumulative depth closely. Subsequently, a minute thickness adjustment is applied across the sequence to ensure a perfect match in total thickness and conservation of the depth of the core. This approach is reasonable where other varved laminated intervals can serve as reasonable surrogates for indistinct sections. We argue this is the case for Columbine Lake, as the distribution of the varvelamination thickness is similar in both cores throughout the sections with distinct varvelaminations (Appendix A Fig. A3). Furthermore, there is no evidence for systematic changes in the mode of deposition in these sections, as the indistinct sections occur throughout both cores, but not always at the same time in the same intervals, and the sedimentary features were mostly the same above and below the indistinct sections, suggesting that the indistinct laminations are due to changes in preservation, not the sedimentation process.~~ .

3.~~7.3~~5 Varve modelling~~Chronology with symmetrical and asymmetrical uncertainty~~

The modified varveR algorithm, which we will refer to as our "varve-only" model, ~~model~~ was used to build two varve chronologies each following a different scenario. In both scenarios, codes 1, 2, and 3 were given over- and under-counting priors. In the first scenario, the priors were symmetrical and based on values found in the literature (Fig. ~~2a;~~2a, ~~e.g.~~e.g., Dräger et al., 2017). This was done to produce a chronology that would resemble the conventional varve chronology construction and allow for comparison. However, due to missing or indistinct varves, varve chronologies are often subject to under-counting (Tian et al., 2005; Żarczyński et al., 2018). Because some of the ~~varve~~lamination**s** in ~~this~~ Columbine ~~lake~~ Lake are thin and ~~often~~ lack~~ed~~ clarity in their appearance, ~~we considered a symmetrical prior to be unrealistic for Columbine Lake. A~~a prior shifted towards under-counting may be ~~was deemed~~ more realistic for lamination code 2 ~~representative~~. The lamina associated with lamination code 3 are indistinct, and we have no reasonable *a priori* estimates of over- or under–counting probabilities. ~~Therefore~~To accommodate these informed priors, in a second scenario~~,~~ we assigned wider symmetrical priors for code 1, wide and~~r~~ asymmetrical priors for code 2, and ~~assigned~~ an uninformed ~~asymmetrical~~ prior for code 3 (Fig. 2b). This expanded

Formatted: Font: Italic

~~version of varveR~~algorithm incorporates uncertainty pertinent to ~~varve~~lamination quality, ~~inter-site~~~~intra-site~~inter-core variation, and expert judgment (Fig. 3).

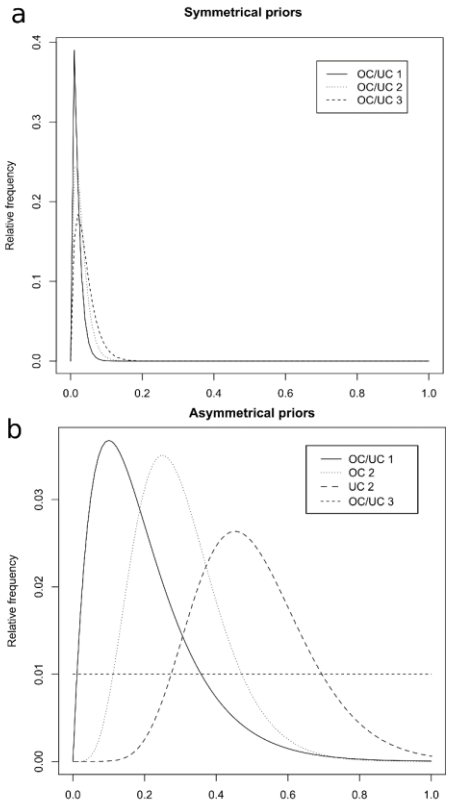

Figure 2. ~~Varve~~Lamination quality codes and their associated under- (UC) and over-counting (OC) gamma distribution priors for (a) symmetrical and (b) asymmetrical ~~varveR~~priors.

~~3.8 Varve chronology verification~~

~~A varve-based age-depth determination should must be cross-checked with other independent dating methods to (1) support the interpretation of varve~~lamination~~s as annual and (2) to identify systematic errors (Ojala et al., 2012; Zolitschka et al., 2015).~~

~~To do so, the varveR~~varve-only model ~~and integrated model output is depth-calibrated and displayed as age-depth curves. Then, the near-surface counts are compared to radionuclide (^{137}Cs and ^{210}Pb) based age-depth models that use conventional CRS and CFCS and Plum, a Bayesian approach to ^{210}Pb dating (Sec. 3.4). The full sequence is compared to a Bayesian radiocarbon age-depth model. All comparisons are made using the dated core (COL17-3).~~

3.~~9~~ ~~6~~ Varve and radiometric chronology integration

Bayesian statistics provide the opportunity to combine different chronological data and their uncertainty (e.g.~~,~~ Buck et al., 2003) as well as information regarding the sedimentation process (e.g.~~,~~ Blockley et al., 2008) by informing priors (Brauer et al., 2014). Here we use Bayesian learning to update prior estimates of the counting uncertainties for each observer given the constraints from the independent radiometric age-depth model. Then, we combine the model produced from each observer into ~~a master~~ one chronology.

Our Bayesian framework uses a custom Gibbs sampler to estimate posterior~~improve on the prior estimates of likelihood probabilities~~ distributions of over- and under-counting ~~described~~ probabilities for each lamination code~~the varveR model~~. The Gibbs sampler is initialized using the prior estimates of over- and under-counting used in the asymmetrical ~~varveR~~varve-only model (Fig. 2b). The sampler updates using an objective function that calculates the likelihood of a proposed varve chronology given the radiometric ages and their probability distributions. We assume the probabilities associated with ~~varve~~lamination quality codes 1 and 2 are best described using gamma distributions and must fall between 0 and 1. For algorithmic efficiency, we loosely impose the assumption that proposed adjustments that increase over-counting rates should be balanced by decreases in under-counting rates, although overall reductions in both over- and under-counting are possible and do occur. ~~The output of the log objective function is the product of the age probabilities of all radiometric samples and the over- and under-counting likelihood of all varve~~lamination ~~quality codes. The higher the output value, the closer the improved varve count is to the maximum likelihood of the product of the radiometric ages. The Gibbs sampler innovates on the previous over- and under-counting probabilities with each iteration if by adjusting with a small random number from a normal distribution, if there is an improvement in the output of the log objective function (i.e. a higher value).~~ We ran the Bayesian algorithm independently for each of the three observers until the objective values stabilized (~100 iterations), then removed the burn-in and thinned the parameter chain to keep 1000 values. Finally, for each observer, we select the parameters corresponding to the 300 highest objective values and combine them into combined posterior distributions. These posterior distributions on the counting rates are ~~then~~ used to ~~drive~~ calculate an ensemble of updated ~~varveR model~~varve counts and produce a master chronology that effectively combines the radiometric age-depth model and the ~~varve~~lamination measurements from all observers (Fig. 3) which we will refer to as the "integrated model".

3.7 Varve chronology verification

A varve-based age-depth determination must be cross-checked with other independent dating methods to (1) support the interpretation of laminations as annual and (2) to identify systematic errors (Ojala et al., 2012; Zolitschka et al., 2015). As discussed in section 3.4, we do not aim to verify that all of the observed ~~lamina~~laminae are annual, rather that our model, represents an ~~annually laminated~~annually laminated depositional regime, with appropriate uncertainties. To do this, we examine our varve-only and integrated model outputs as age-depth curves. Then, the near-surface counts are compared to radionuclide (^{137}Cs and ^{210}Pb) based age-depth models that use conventional CRS and CFCS and Plum, a Bayesian approach to ^{210}Pb dating (Sec. 3.42). The full sequence is compared to a Bayesian radiocarbon age-depth model. All comparisons are made using the dated core COL17-~~3~~3.

Formatted: Not Highlight

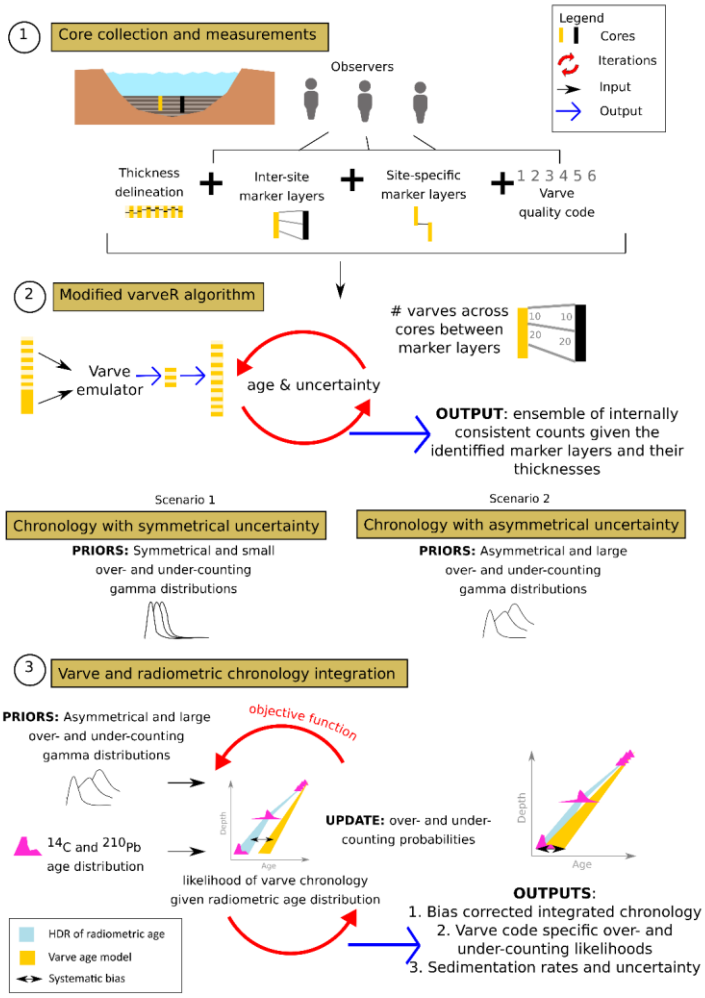

Figure 3. Schematic of the approach used in this study. (1) Gathering raw measurements of ~~varve~~lamination thickness, counts, and marker layers for each core and each observer. (2) Using ~~a modified version of~~our ~~varveR~~varve-only model to produce a chronology following scenario 1 (symmetrical and literature-derived likelihoods of over- and under-

counting) and scenario 2 (asymmetrical and larger likelihoods of over- and under-counting). (3) Integrating radiometric information into the varve chronology by updating the prior likelihoods of over- and under-counting in an objective function. The posteriors of the *n*th best function output are used to run an updated ~~varveR~~varve-only model and produce the final chronology that minimizes systematic bias and quantifies uncertainty related to misidentifying marker layers, observer bias, and ~~varve~~lamination quality and outputs sedimentation rates with uncertainty.

4 Results

4.1 Sediment profile

Columbine Lake sediments were previously described generally by Arcusa et al. (2019) and more detail is provided here. The sediments ~~contain five stratigraphic units~~are composed of minerogenic, laminated silts and clays ranging in color from grey to reddish-brown to orange (Fig. 4~~a and Fig. 5~~). Three of the four cores showed identical sediment profiles, meeting the requirement of reproducibility, but only COL17-2 and COL17-3 captured an intact sediment-water interface and laminations (Appendix A Fig. A1). Sediment between 141-126 cm (core depths from COL17-2) are characterized by massive grey clay-sized sediment. Sediment between 123-72 cm contain ~~lamination~~contains poor quality laminations frequently interspersed with indistinct sections. The sections of indistinct ~~varve~~lamina preservation generally correlate across the parallel cores, although are more prevalent in core COL17-2 (Fig. 4a). ~~laminalamination~~ Sediment between 72-12 cm contains laminations of average clarity with indistinct sections (Fig. 4a). ~~The sections of indistinct varvelaminations generally correlate across the parallel cores, with exceptions.~~ Sediment between ~~laminalaminationlaminalamination~~12-0 cm contains well-defined laminations as well as massive fine silt layers. The lower part (12-2 cm) contains fine, grey, ~~varve~~laminae, ~~laminations~~ interspersed by two massive layers. The two massive light brown layers are both in core COL17-2, with core COL17-3 only containing the youngest of the two. Core COL17-3 contains a layer of indistinct laminations that cross-correlates with the oldest of the two COL17-2 massive layers suggesting the layers are composed of poorly preserved ~~varve~~lamina ~~laminations~~ as opposed to single massive bed deposited rapidly. The upper part (0-2 cm) contains thicker bright orange ~~varve~~lamina ~~laminations~~ just below the sediment-water interface.

~~4.1.1 Units 5 and 4~~

~~Unit 5 (141-126 cm; depths in core COL17-2) is characterized by massive grey clay-sized sediment and lithogenic indicators (Si, Ti, K, Al, Rb, MS) are typically high and covary (Appendix A Fig. A4, A5 and A6). Unit 5 contained missing data so could not be included in the PCA (Fig. 5). The transition between units 5 and 4 is marked by a large and rapid increase in the redox element Mn, along with an instantaneous increase in Mn/Fe (Appendix A Fig. A5). Unit 4 (123-108 cm) is the first unit to contain laminations and correspond to the most elevated Fe and P. This unit contains type 1 varves.~~

Formatted: Font: Italic

Formatted: Not Highlight

Formatted: Not Highlight

Formatted: Not Highlight

Formatted: Not Highlight

~~4.1.2 Unit 3~~

~~Unit 3 (105-75 cm) contains poor quality laminations frequently interspersed with indistinct sections. The sections of indistinct varve preservation generally correlate across the parallel cores, although are more prevalent in core COL17-2 (Fig. 4). Unit 3 is characterized by type 1 varves.~~

~~4.1.3 Unit 2~~

~~Unit 2 (72-12 cm) contains laminations of average clarity with indistinct sections (Fig. 4a). The sections of indistinct varves generally correlate across the parallel cores, with exceptions. Type 1 varves are present, although type 2 varves start to appear intermittently in core COL17-2. The break between units 3 and 2 coincides with a general shift from type 1 to type 2 that is evident both in the thin section microfacies analysis and the hierarchical clustering. Unit 2 sees a small but significant decrease in magnetic susceptibility and Fe compared to unit 3 (Appendix A A4 and A5).~~

~~4.1.4 Unit 1~~

~~This unit (12-0 cm) contains well-defined laminations as well as massive fine silt layers and can be further split into two sub-units. The lower sub-unit (12-2 cm) contains fine, grey, type 3a and b varves interspersed by two massive layers. The two massive light brown layers are both in core COL17-2, with core COL17-3 only containing the youngest of the two. Core COL17-3 contains a layer of indistinct laminations that cross-correlates with the oldest of the two COL17-2 massive layers suggesting the layers are composed of poorly preserved varves as opposed to single massive bed deposited rapidly. The other sub-unit (0-2 cm) contains thicker bright orange type 3b varves just below the sediment-water interface. Organic and biogenic (percent organics, biogenic silica, and green pigments as indicated by the index of RABD660) abundance increase to their highest levels in the top sub-section (Fig. 5, Appendix A Fig. A5), indicating increased lake productivity. Some heavy metals (Zn, Ag) also increase to their maximum levels (Appendix A Fig. A4).~~

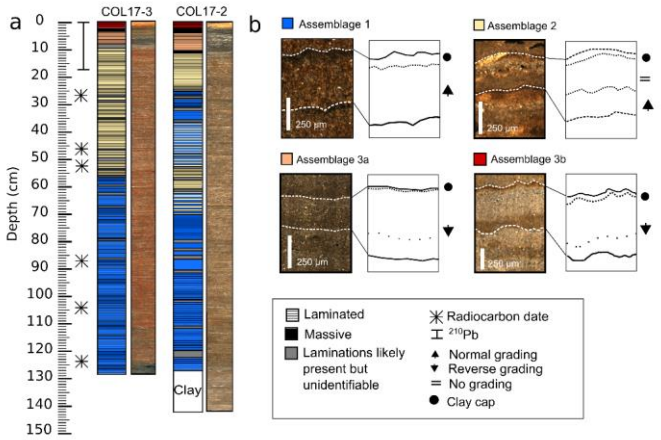

Figure 4. Sediment ~~, proxy,~~ and ~~varve~~lamination profiles. (a) Lithostratigraphy and location of radiometric samples of cores COL17-3 and COL17-2. Images are true color. The base of COL17-3 is black because the oxidized red crust has been scraped off. ~~MS = magnetic susceptibility, BSi = biogenic silica. Other proxies are shown in Appendix A A5.~~ (b) Microscopic thin section examples of ~~varve lamination types~~assemblage 1, 2, and 3. ~~(c) Microscopic sub-lamination grain size analysis of varve types 1, 2, and 3b.~~

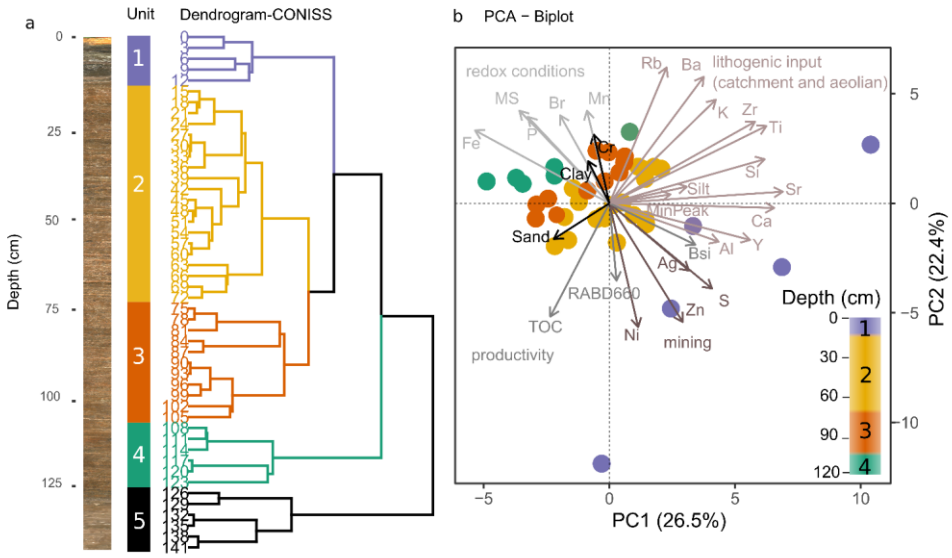

~~**Figure 5. Statistical analysis of proxy data from core COL17-3. (a) A constrained dendrogram with significant clusters representing the stratigraphic units (1-5) color-coded and applied to the sample depths used in the (b) Principal Component Analysis (PCA) biplot for reference. The first two principal components explain 48.9% of the variability. PC-variables grouped by indicator type have different colors. The image of the core is presented for context. PCA loadings and scores can be found in Appendix A Fig. A7.**~~

4.2 ~~Varve~~ Lamination ~~type~~ description

The examination of thin sections revealed complex microfacies that repeat within each lamination, indicative of a rhythmic change in the depositional environment. Moreover, comparison to radiometric measurements demonstrate this rhythmic layering is annual (Sect. 4.6). Therefore, the sediment is described here as true non-glacial clastic ~~varves~~lamina. Three ~~main types~~ assemblages of clastic ~~varves~~ lamina are further sub-divided based on their internal structure (Fig. 4b). ~~Type~~ Assemblage 1 is composed of typical couplets of silt and clay, ~~type~~ assemblage 2 couplets are interrupted by a third coarser grained sub-laminae, and ~~type~~ assemblage 3 couplets are inversely graded, with thinner (3a) or thicker (3b) clay-sized caps and darker (3a) or lighter (3b) color laminae (Fig. ~~4c~~4b).

4.2.1 ~~Type~~ Assemblage 1

~~Type~~ Assemblage 1, most common in the deepest half of the sequence, consists of couplets identified by color and grain size. The ~~bottom~~ bottom ~~part~~lamina ~~, lithozone I,~~ is characterized by ungraded or fining upward grading of light reddish-brown sediment ~~with grains that measure 5-15 µm~~ (Fig. 4b~~c~~). The top ~~part~~lamina ~~, lithozone II,~~ is a ~~a~~ fine-grained, dark-brown clay-rich cap ~~with grains consistently < 5 µm~~ (Fig. 4b~~e~~). The contact between ~~lithozones I and II~~them is generally ~~gradual~~sharp.

4.2.2 ~~Type~~ Assemblage 2

~~Varve~~~~Lamination type~~Assemblage 2 is most common in the top half of the sequence. Like assemblage 1, assemblage 2 bottom lamina is silt-sized and inversely graded. The top lamina is terminated with a dark reddish-brown clay-sized cap. However, the couplets are ~~and consists of couplets~~often ~~(lithozone I and II)~~ interrupted by coarser-grained ~~(25-40 µm)~~ matrix-supported ~~sub~~ laminae, which are composed of plagioclase, quartz, and oxides, as identified under polarized microscope light ~~(lithozone III)~~. The contact between the bottom lamina and this lamina is ~~An~~ erosional ~~contact separates lithozone I from III, which is composed of plagioclase, quartz, and oxides, as identified under polarized microscope light~~. ~~Like type 1 varves~~lamina, ~~type 2 varves~~ lamina ~~are terminated with a dark reddish-brown clay cap (<5 µm, lithozone II).~~

4.2.3 ~~Type~~ Assemblage 3

~~Type~~ Assemblage 3 ~~varve~~~~laminas~~ are found exclusively at the topmost part of the sequence and can be sub-divided into ~~varve~~~~lamination type~~assemblage 3a and 3b. The deeper~~st~~ of the two in the sediment sequence, ~~type~~ assemblage 3a, is generally thicker and contains ~~lithozone IV. Lithozone IV is characterized by~~ a reverse grading of fine and dark grains at the bottom to coarse and light sediment at the top (Fig. 4b~~c~~). ~~Lithozone~~ This lamina~~IV~~ is followed by a thin and sometime non-existent ~~lithozone II~~clay-sized cap. Finally, at the topmost part of the ~~cores~~ sediment sequence is ~~varve~~~~lamination type~~assemblage 3b, similar in composition to ~~varve~~~~lamination type~~assemblage 3a. The difference is a strongly pronounced clay-sized cap ~~(lithozone II)~~. Both assemblage 3a and b have a sharp change in color from dark to light. ~~Varve~~~~Lamination type~~Assemblage 3 differs from ~~type~~ assemblage 2 by its reverse grading~~because the coarsest grains appear gradually within lithozone IV rather than abruptly in lithozone III. Lithozone IV in varve~~lamination ~~type 3a and b also gradually change in color from dark to light.~~

4.3 ~~Varve c~~Counts, thicknesses, and quality

~~Varve~~ Lamination thicknesses, excluding ~~varves~~ lamina of quality code 4, 5, and 6, are similar for each core (Table 1), with a combined mean and standard deviation of 0.5 ± 0.~~05~~3 mm. Thicker ~~varve~~laminae~~s~~ were found in COL17-3 (4.5 mm) compared to COL17-2 (2.81 mm). ~~Varve~~Lamination quality varied greatly between observers ~~was generally higher at the top of the two cores (code 1)~~ and fluctuated between moderate and poor quality throughout (Fig. ~~6~~5). The minimum thicknesses of 0.04 mm measured in COL17-2 may appear small, but the algorithm does not allow for a minimum value that is smaller than any measured lamination.

Lamination observations were integrated into a varve count ensemble using the varve-only model. With the symmetrical ~~varveR~~varve-only model, cores COL17-2 and COL17-3 contain a total of 2466 (highest probability density region: 2075-2880) and 2380 (1999-2710) varves, respectively (Table 2, Fig. ~~7~~6). This amounts to a cumulative uncertainty of -391/+414 varves (-17/+15 %) for COL17-2 and -381/+330 (-17/+13 %) for COL17-3. With the asymmetrical ~~varveR~~varve-only model, the mean total varve count increases by 300-400 varves to 2865 (1417-3923) for COL17-2 and 2740 (1394-3742) for COL17-3 although the cumulative uncertainty also increases to -1448/+1058 varves (-68/+31 %) and -1346/+1002 varves (-65/+31 %), respectively.

Table 1. Summary statistics ~~for varve thicknesses~~ based on the average of all observers' measurements, excluding intervals of indistinct laminations. Total varve counts indicate output of the symmetrical ~~varveR~~varve-only model.

Core	COL17-2	COL17-3
Length of ~~varved~~ laminated sequence (cm)	127	123
Mean total varve count	2466	2380
Median varve thickness (mm)	0.43	0.47
Minimum~~.~~ varve thickness (mm)	0.04	0.05
Maximum~~.~~ varve thickness (mm)	2.81	4.50
Mean varve thickness (mm)	0.49	0.52
Standard deviation varve thickness (mm)	0.28	0.29

Formatted: Keep with next
Formatted: Keep with next
Formatted: Keep with next
Formatted: Keep with next
Formatted: Keep with next
Formatted: Keep with next
Formatted: Keep with next
Formatted: Keep with next

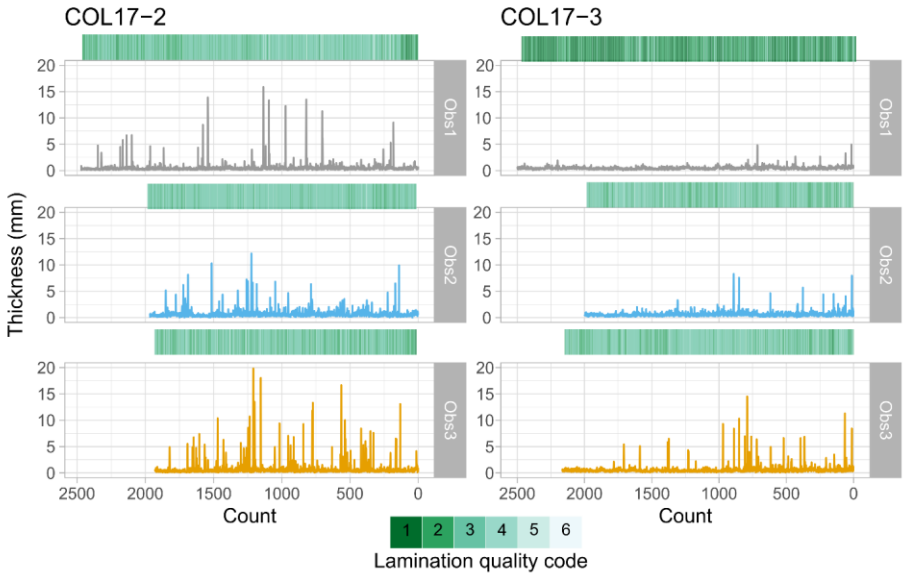

Figure 65. Observer measurements of ~~varve~~ lamination thicknesses (lines) and quality (heatmaps) for cores COL17-2 and COL17-3.

Table 2. Comparison of observer and core-specific varve ages based on the symmetric and asymmetric ~~varveR~~ varve-only model as well as the integrated model. HDR = highest probability density region.

	COL17-2				COL17-3			
Symmetrical ~~varveR~~varve-only model	Obs 1	Obs 2	Obs 3	**Average**	Obs 1	Obs 2	Obs 3	**Average**
Ensemble mean total count (varve years)	2749	2171	2478	**2466**	2616	2103	2419	**2380**
HDR (2.5-97.5%)	2614-2911	2037-2320	2351-2617	**2033-2847**	2498-2739	1958-2249	2283-2543	**1999-2710**
Difference from average (%)	+10.9	-12.7	+0.5	**23.6***	+9.4	-12.4	+1.6	**21.8***
Asymmetrical ~~varveR~~varve-only model								
Ensemble mean total count (varve years)	3107	2590	2898	**2865**	2899	2506	2813	**2740**
HDR (2.5-97.5%)	2015-4182	1233-3733	1756-3864	**1417-3923**	2161-3717	1227-3595	1699-3811	**1394-3742**
Difference from average (%)	+8.1	-10.1	+1.1	**18.2***	+5.6	-8.9	+2.6	**14.5***
Integrated model								
Ensemble mean total count (varve years)	3470	3309	3227	**3308**	3095	3178	3138	**3137**
HDR (2.5-97.5%)	3098-4075	3139-3493	3091-3370	**3091-3970**	2624-3414	3036-3333	2968-3309	**2753-3375**
Difference from average (%)	+4.8	0	-2.5	**7.3***	-1.3	+1.3	0	**2.6***

*) Indicates the observer agreement as the range in the percentage difference from the mean

Formatted: Left

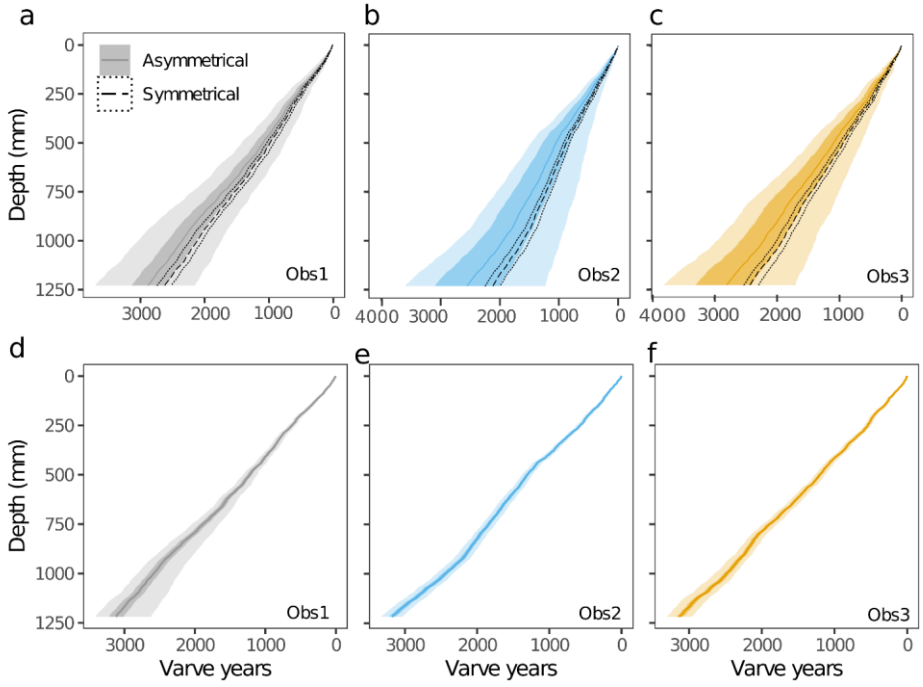

Figure ~~7~~6. Comparison of ~~original~~ varve-only modeled counts by (a and d) observer 1, (b and e) observer 2, and (c and f) observer 3 for dated core COL17-3. In the top row, the modeled varve counts are shown when using symmetrical (dotted envelop) and asymmetrical (shaded envelop) priors. For the symmetrical uncertainty, the median (dashed line) and the 97.5% (dotted region) high density regions are depicted. For the asymmetrical uncertainty, the median (darkest line), 75 (darkest shaded region), and 97.5% (lightest shaded region) high density regions are depicted. In the bottom row, the integrated varve and radiometric models are shown.

4.4 Observer-related uncertainty

Three observers independently ~~measured~~ delineated the ~~varves~~ lamina of cores COL17-2 and COL17-3 in one ~~in three separate~~ transect each~~s~~ (~~Table 2~~Fig. A2). The cumulative uncertainty of each observer to the mean was ~~slightly~~ higher for asymmetrical than symmetrical ~~varveR~~varve-only model. The uncertainty varied between 0.5 % (observer 3 COL17-2) and 12.7 % (observer 2 COL17-2). The ~~Asymmetrical~~ asymmetrical ~~varveR~~varve-only model suggests more under-counting for observers 2 and 3

and more over-counting for observer 1 (Fig. ~~7~~6). However, segment differences are both positive and negative for all observers, indicating that systematic bias may not be an issue (Appendix A Table A1). The observer agreement is high for minimum thickness but low for maximum thickness (Appendix A Table A2). Observers disagreed on the number of indistinct sections, pointing to the subjectivity of varve delineations and confidence levels. Agreement on varve quality between observers is low (Fig. ~~6~~5), highlighting the challenge of identifying lamina in some sections of the sequence, and indicating further subjectivity. Sections with thicker varves generally correlate across all observers such as between the varve years of 0-100 and 750-1000 in COL17-3 or between the varve years of 1000-1500 in COL17-2 (Fig. ~~6~~5).

4.5 Marker layer uncertainty

As marker layers were assigned by each observer individually, they ~~may~~ do not always agree between observers. The identification of marker layers is a key additional source of uncertainty that is modeled in our approach. Consequently, ~~Thus,~~ the varve count between marker layers, or segment count, in each core indicates a combination of ~~inter-site~~intra-siteinter-core variability due to the sediment quality and observer judgment (Appendix A Table A1). The largest segment difference was 110 % (172 years) for one observer which cannot be explained by marker layer misidentification alone. Instead, it is indicating that one observer identified more indistinct sections than the other observers for one of the sites.

4.6 Independent validation

The topmost part of core COL17-3 was dated with two independent radionuclide profiles. The ^{210}Pb activity in Columbine Lake exhibits a gradual downcore decline that reaches equilibrium around 50 Bq kg^{-1} below 8 cm (Fig. ~~8a~~7a). The age at the base of the radionuclide measurements (12 cm) modeled by conventional methods for CRS and CFCS vary widely (Fig. ~~8c~~7c): CRS reaches 1883 ± 14 CE whereas CFCS comes to 1940 ± 13 CE. In comparison, the Bayesian solution has a wider, but likely more realistic uncertainty at 12 cm yielding a median age of 1784 CE with a 95 % highest density region of 1866-1679 CE. Although the range of the uncertainty is more realistic, the ages themselves may not: Pb becomes unsupported by 8 cm (~1800 CE). The ^{137}Cs activity shows a single peak at 3.25 cm (Figure ~~4.8B~~7b) which we attribute to the 1963 CE fallout from nuclear weapon testing. The peak's depth appears younger by 20 to 30 years in the ages modelled from the ^{210}Pb~~lead~~ profile: CRS indicates a year of 1996 CE, for CFCS it is 1998 CE, and 1984 CE for Plum. Despite this discrepancy, it is very unlikely that the peak at 3.25 cm is related to Chernobyl fallout; such a peak is almost never found in North America (Lima et al., ~~2005; Omelchenko~~2005; Omelchenko et al., 2005; Munoz et al., 2019), and we are not aware of a Chernobyl-related ^{137}Cs peak reported in lake sediment in the western United States. ~~The peak's depth appears younger by 20 to 30 years in the ages modeled from the lead profile: CRS indicates a year of 1996 CE, for CFCS it is 1998 CE, and 1984 CE for Plum.~~

A total of six radiocarbon dates ranging in age from 20 to 310 years were used to model the age profile of Columbine Lake sediment (Table 3). ~~Three dates were previously reported by Arcusa et al. (2019) (UCI 196901, UCI, 190157, and UCI 188317) for a mixture of small insects and plant fragments dated with a calibrated-age uncertainty ranging from 20 to 310 years.~~ One

Formatted: Superscript

Formatted: Superscript

Formatted: English (United Kingdom)

new date was discarded as it returned a modern age (IonPlus 3528). Two more dates (IonPlus 3529 and IonPlus 3530) were measured on a mixture of plant fragments, bark, and aquatic insects due to the paucity of organic material found in the sediment. The uncertainty of the two new dates ranged from 72 to 76 years. The calibrated basal age at 124.5 cm is 2997 ~~(95.4 % probability: 3073-2888)~~ yr BP (95.4 % probability: 3073-2888).

To verify the annual nature of the couplets in Columbine Lake, we compare the topmost part of the ~~varveR~~varve-only model model with symmetrical priors to the ^{137}Cs ~~chronomarkers~~ peak and the entire sequence to the radiocarbon profile (Fig. ~~8c~~ 7c and f). Cesium-137 is used for comparison because of its lower uncertainty, as opposed to the ~~lead~~ ^{210}Pb age models which are not in close agreement among themselves. The varve count and uncertainty by all three observers show a high agreement with the ^{137}Cs peak, suggesting the couplets are annual. The whole sequence agrees generally well with the radiocarbon profile, particularly in the top 25 cm. Uncertainty surrounding the varve count increases downcore and the varve counts no longer overlap with the radiocarbon uncertainty ~~to a depth of~~below ~~60~~ 50 cm. The basal radiocarbon age is older than the mean age estimated by both symmetrical and asymmetrical ~~varveR~~varve-only models by 600 and 250 years, respectively. The cumulative uncertainty of asymmetrical ~~varveR~~varve-only model encompasses the radiocarbon basal age, whereas the symmetrical ~~varveR~~varve-only model does not. ~~Counts from observer 1 have the most counts, and are systematically closer to t~~The radiocarbon age estimate is the closest to the estimate from observer 1. The comparison with radiocarbon also serves to identify systematic biases. ~~which i~~In the case of Columbine Lake, the ^{14}C data suggest that the varves are systematically under-identified. ~~tend towards under-counting when using symmetrical priors and possibly over-counting when using asymmetrical priors.~~

Formatted: Superscript

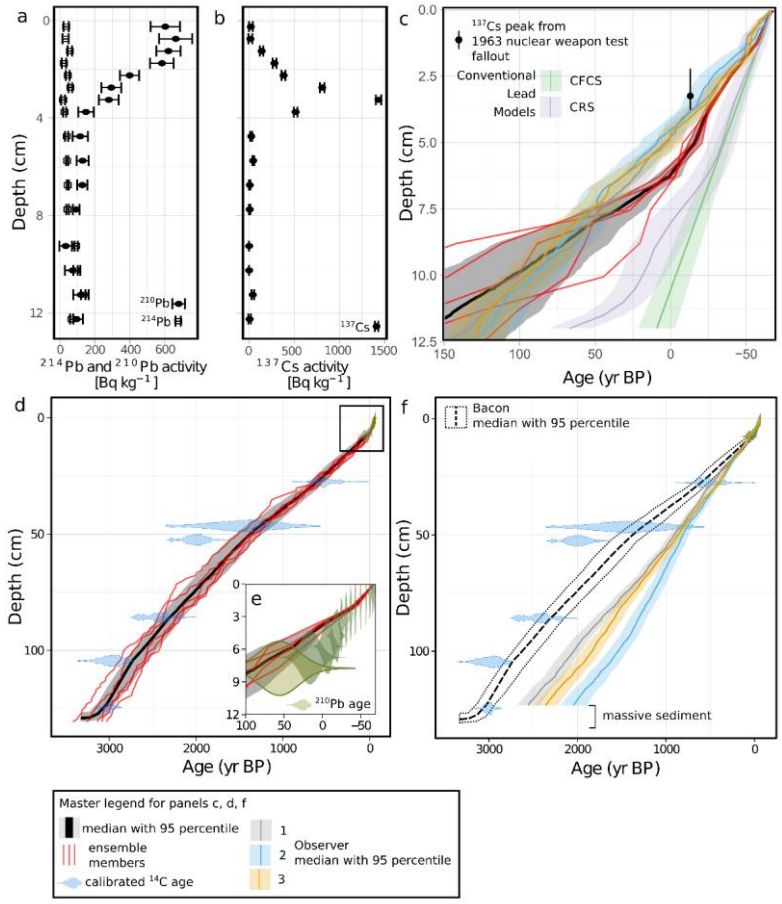

445 **Figure ~~8~~7. The chronology of Columbine Lake core COL17-~~3~~3. ~~based on~~ (a) ~~lead~~ ^{210}Pb raw measurements~~and~~. (b) ^{137}C~~caesiums~~ raw measurements. (c) Comparison of lead models (green = CFCS, purple = CRS) and the caesium peak of the 1963 nuclear weapon test to the radiometric model (black/red/grey = Plum and Bacon) and to the varve-only model (light grey/blue/yellow = varve-only model). Plum is a statistical framework that models lead-derived ages with more realistic uncertainties.~~is seamlessly combined with (c, d) radiocarbon samples using the Bayesian models of Bacon~~

450 ~~and (e) Plum. Plum performs better than (c) conventional lead models of CFCS and CRS when compared to the 1963~~

Formatted: Superscript

~~^{137}Cs fallout peak. The age-depth models counted by three observers and modeled by varveR with symmetrical priors agree well with the fallout peak indicating the rhythmic laminations are annual. Compared to (f) radiocarbon, underestimations in the varve counts appear to accumulate downcore.~~

(d) Radiometric model produced from combining the Bacon-derived radiocarbon age-depth model with the Plum-derived lead age-depth model. Black and grey represent the median age with 95th percentile. The red lines represent five randomly selected ensemble members. Blue probability distribution functions represent the calibrated radiocarbon ages. (e) Plum-derived lead age-depth model. Brown probability distribution functions represent the sampled ^{210}Pb ages. (f) Comparison of the radiometric model (Bacon and Plum combined) to the varve-only models for each observer. Panel (c) shows the same area of the graph as panel (e).

Formatted: Justified

Formatted: Superscript

Table 3. Uncalibrated and calibrated radiocarbon dates.

Lab ID	Depth[a] (cm)	Material	^{14}C Age (^{14}C yr BP)	Error (± 1sd yr)	From[b] (cal. yr BP)	To[b] (cal. yr BP)
UCI 196901	27.5	Insect wing	520	100	671	319
UCI 190157	46.5	Bryophyte twig, Daphnia ephippia	1510	310	2146	790
IonPlus 3527	52.5	Daphnia ephippia, insect armour	2045	69	2299	1798
IonPlus 3528[c]	77.75	Daphnia ephippia, charred twig	~~-~~ ~~935~~112.37	60	-	-
IonPlus 3529	85.75	Daphnia ephippia, charcoal	2365	72	2710	2160
IonPlus 3530	104.5	Daphnia ephippia, bark	2845	76	3170	2777
UCI 188317	124.5	Bryophyte twig, Daphnia ephippia	2875	20	3073	2888

[a] Mid-point depth of 1-cm-thick sample

[b] Two sigma range calibrated with IntCal20 curve

[c] Value is given in percent modern carbon (fraction modern multiplied by 100). Fraction modern for this sample is 1.1237. Age not used because returned modern.

4.7 Varve and radiometric data integrated model

One integrated model was created for each observer. The integrated models updated the prior estimates of the counting uncertainties given the constraints from the independent age model and given each observer's varve thicknesses, varve quality designation, and marker layer identification. The models sampled the probability space for 50,000 iterations and the burn-in occurred rapidly in < 100 steps (Appendix A Figure ~~A8~~A4). The integrated models result in similar cumulative uncertainty to symmetrical ~~varveR~~varve-only model but are much smaller than the uncertainty estimated by asymmetrical ~~varveR~~varve-only model (Fig. ~~7~~6 and 8). The integrated models also converge more: the difference in the basal age between observers shrinks to 2.6 %, down from 21.8 % in the symmetrical ~~varveR~~varve-only model. The posterior likelihoods of over- and under-counting are larger than the symmetrical priors (Fig. 2 compared to Appendix A Figure ~~A9~~A5). They also varied with each varve quality code and with each observer (Appendix A Figure ~~A9~~A5). The integrated models were more successful at correcting for over- and under-counting for observers 2 and 3 than observer 1 as seen from the more symmetrical cumulative uncertainty for those observers (Appendix Fig, ~~A8~~A4).

Each observer's integrated model was combined into one single integrated model, which hereafter is referred to as the 'integrated model'. The integrated model cumulative age extends by 3137 (3375-2753) varve years or 1120 (1358-736) BCE corresponding to a cumulative uncertainty of -384/+238 years (-13/+7 %) (Table 2). The cumulative mean age is older than symmetrical and asymmetrical ~~varveR~~varve-only model and the independent model. However, the HDR encapsulates the mean age of the radiometric model (Fig. ~~9b~~8b). The greatest deviation between the independent model and the integrated model occurs between 30 and 80 cm depth where indistinct sections are most frequent (Fig. ~~9b~~8b). The cumulative uncertainty in the integrated model is lower than asymmetrical ~~varveR~~varve-only model and similar to the symmetrical ~~varveR~~varve-only model.

The posterior probabilities of over- and under-counting consistently increase ~~from~~ for ~~varve~~lamination quality codes 1 ~~to 3~~and 2, consistent with the priors, and theory, as we'd expect the highest quality lamina to be identified correctly most frequently. The ~~modes of the~~ posterior probabilities are ~~higher~~ of under- or over-counting are higher than the priors ~~expectations~~ for all ~~varve~~ lamination quality codes except for the probability of under-counting code 2 ~~except for the likelihood of over-counting code 3~~ (Fig. ~~9a~~8a). The probability of over- and under-counting is similar for varve code 1, with a slight tendency for more under-counting (11 % vs 14 %). Furthermore, the probability of over- and under-counting varve code 2 is the same (41 % vs 40 %). In contrast, the likelihood of over-counting varve code 3 is much smaller than the likelihood of under-counting (10 % vs 88 %). However, the distribution of the likelihood of over-counting is much wider than for other ~~varve~~ lamination quality codes indicating this parameter has the least influence on the iterative improvements made by the Gibbs sampler. More under-counting appears with deeper sediment due to the dominance of poorly preserved sediment identified as lamination ~~varve~~ quality code 3. Similar posterior probabilities resulted from re-running the integrated model with smaller asymmetrical uncertainty.

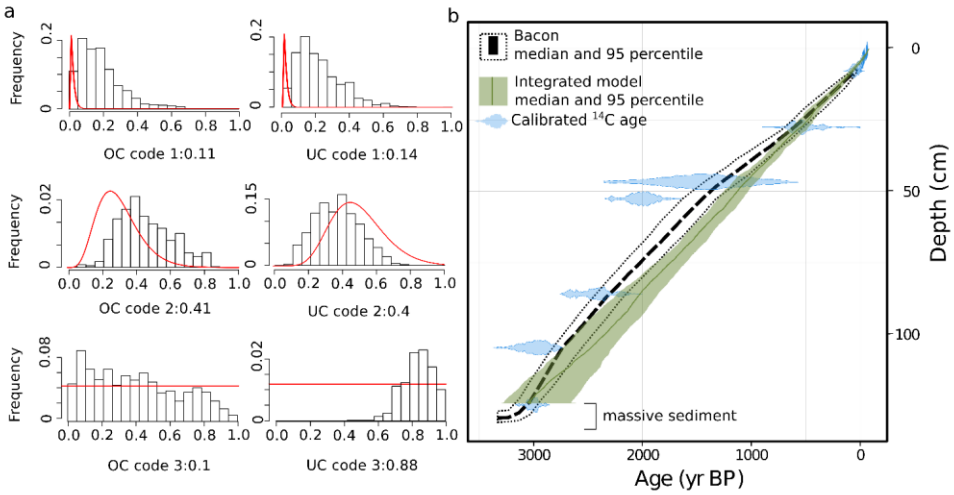

Figure 98. Integrated varve-radiometric model. (a) Over- and under-counting posterior distributions for the integrated model for each lamination ~~varve~~ quality code (1, 2, 3). (b) Age-depth model comparison of the independent (Bacon) age model and the integrated model. OC: over-counting. UC: under-counting. ~~Blue line indicates the mode of the posterior distributions.~~ Red line indicates ~~the mode of~~ the prior distributions.

Formatted: Font: Bold

4.8 Sedimentation rates

The estimated sedimentation rate and its uncertainty varied by method and observer (Fig. ~~10a~~9a). Average rates are similar for all varve-only models with estimates of 0.51 mm/yr (HDR: 0.12-1.45) in the symmetrical ~~varveR~~varve-only model, 0.44 mm/yr (HDR: 0.08-1.76) in the asymmetrical ~~varveR~~varve-only model, and 0.42 mm/yr (HDR: 0.08-1.30) in the integrated model. ~~In contrast, rates are doubled on average and higher more frequently in the independent model (0.83 mm/yr, 0.11–3.63) (Fig. 10).~~The long-term sedimentation rates from the independent model are similar (0.41 mm/yr, HDR: 0.39-0.43). In detail, because of the way sedimentation rates are calculated by the program Bacon, the time increments vary, leading to the higher mean sedimentation rate on average evident in Fig. 9. ~~The uncertainty range in the varve models is half of that in the radiometric model.~~The summary of sedimentation rates shows relatively consistent multimodal distributions for all models and all observers (Fig. 9a). However, no such modes are observed from the raw measurements (Appendix A Fig. 3) suggesting this is a feature that appeared during the modelling. They may represent different modes of sediment deposition or artifacts, but further investigation would be necessary.

Sedimentation rates appear more stable throughout the late Holocene in the integrated model than for the radiometric model (Fig. ~~10b~~9b). Periods of higher sedimentation rates occur in the integrated model in the last 100 years, 400-500 BP and 2000-2200 BP. Only the last 100 years of the integrated model shows a similar although subdued trend to the radiometric model. Although there are significant discrepancies in implied~~Furthermore,~~ sedimentation rates between different~~are highly sensitive to the~~ observers in the integrated ~~measurements with relatively little agreement (Appendix A Fig. A10)~~model, the impact of observer differences on the chronology is far less than in either varve-only model (Fig. ~~10~~9; Appendix A Fig. A~~10~~6). As expected, the unifying influence of the radiometric dates reduces the impact of observer biases~~. Those periods of agreement would show lower uncertainty, but uncertainty is relatively stable throughout the record (Fig. 10b).~~, a potential benefit of the approach, especially in sequences that are difficult to delineate and prone to observer bias.

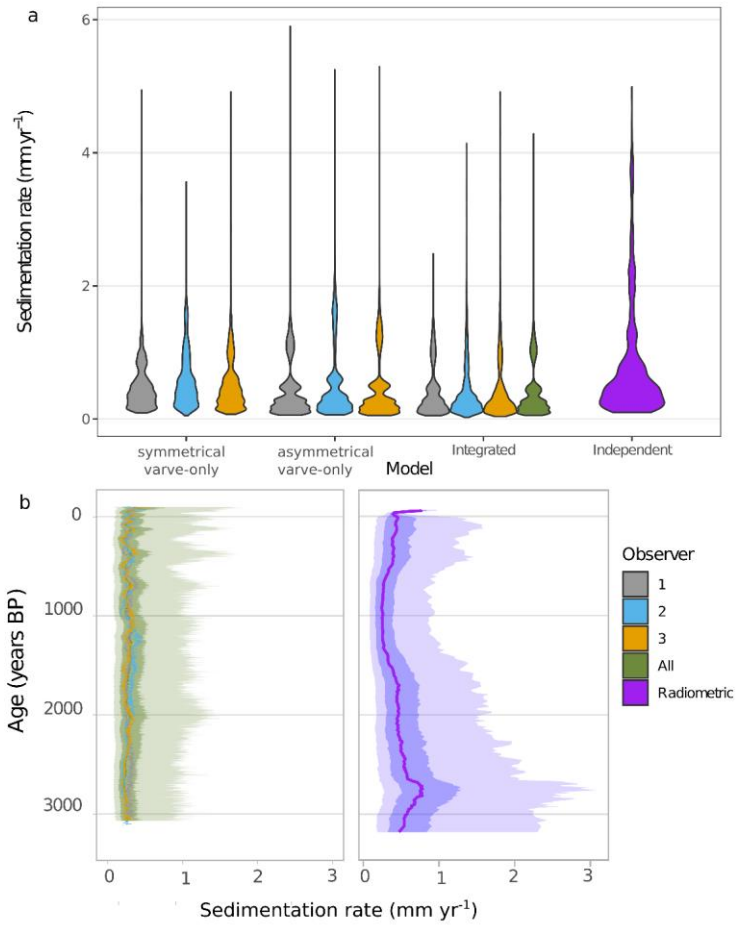

Figure ~~10~~9. Comparison of sedimentation rates. (a) Summary of sedimentation rates calculated with different models and separated by observer. (b) Late Holocene median (thick lines), 75% (darker shading) and 97.5% (lighter shading) highest probability density regions estimates of sedimentation rates calculated by the integrated (left) and radiometric (right) models for the dated core COL17-3. Note the medians of each observer are plotted in the left panel (thick lines).

5 Discussion

5.1 Sources and quantification of uncertainty

Varve chronologies~~, like all sedimentary profiles,~~ contain uncertainties that stem from complex internal structures, poor quality, technical problems, rapid deposition events, and erosion (Ojala et al., 2012). Unlike other sedimentary chronologies, the errors in varve chronologies are propagated by the observer(s) who ~~somewhat~~ subjectively determine what is a varve by "lumping" or "splitting" thicknesses. The sources of uncertainty and their quantification in Columbine Lake are now discussed in turn.

Formatted: English (United Kingdom)

5.1.1 Sediment microstructures

The combination of the complex internal structure, shifting structures through time, and thinness of Columbine Lake varves was likely the most important source of uncertainty (~~Fig. 4b,~~ Sect. 4.2). The complex sub-lamina internal structures of the clastic varves are the primary cause of the large uncertainties in observer identification and delineation. It is also likely that laminations are missing due to erosion. Both would result in the under-counting that is particularly evident when comparing the symmetrical and asymmetrical ~~varveR~~varve-only models to the independent chronology (Fig. ~~8~~6 and 7). The systematic bias is corrected by the integrated model. Additionally, uncertainty in the varve delineation impacts the thickness measurements which propagates into the sedimentation rates (Fig. ~~10~~9). At an average thickness of 0.5 ± 0.05 mm, the uncertainty surrounding the delineation of each varve is likely to be proportionately large because of the image quality and pixel resolution used in this study. Missing laminations and misinterpretation due to complex varve structures are common reasons for imprecision (Ojala et al., 2012).

5.1.2 Sediment quality

Closely intertwined with the sediment microstructures, sediment quality is likely the second-most important source of uncertainty in the chronology as seen from the prevalence of poor varve quality codes (2 and 3) (Fig. ~~6~~5). About 78% of the sediment of COL17-2 and COL17-3 was identified as code 2, 3, and 4, all three designations indicating the observer was less than 80 % certain the thickness delineated was accurate. We report a cumulative uncertainty (-13/+7 %) in the integrated model that is on the higher end of values reported in the literature: a cumulative uncertainty of ±1-3 % is reported in the literature for well-preserved sediment (Ojala et al., 2012) and up to 15 % for unclear, partially disturbed varves in otherwise well-preserved varve sequences (Ojala and Tiljander, 2003; Tian et al., 2005). We also find high estimates of probabilities of over- and under-counting. These uncertainties are not always quantified in the literature, but Ojala and Tiljander (2003) report uncertainties within sections that reach 12 % and indicate more over-counting with depth. Additionally, Fortin et al. (2019) report over- and under-counting estimates of 21.9 and 14.5 %. We find large uncertainty estimates even for the best quality varves in Columbine Lake.

The presence of indistinctly laminated sections was frequently identified in both cores (Fig. 4). The timing of these segments is generally correlated across both cores, with exceptions, suggesting a combination of macro and micro scale processes. We accounted for this uncertainty through varve code 5 by emulating varved sediment. Through this analysis, we found that, on average, more sediment was identified as indistinctly laminated in COL17-2 (25 cm) than COL17-3 (11 cm). In more detail, the identification and thickness of these segments varied between observers suggesting differences in expert confidence and indicating high uncertainty may be surrounding the timing of these segments. As a result, the meaning of these indistinct segments should be interpreted with caution.

5.1.13 Observer judgement

Conventional varve chronology development usually requires multiple observers counting and re-counting until an agreement is found (Fortin et al., 2019) or one observer using multiple counting methods (Żarczyński et al., 2018). Ideally the observers have extensive experience recognizing and delineating varves~~are varve counting experts~~. Nevertheless, all observers bring their biases and an element of ~~These exercises reveal that varve counting has an element of~~ subjectivity, ~~with~~as they have to make choices about ~~observers~~ splitting or lumping varves, which is especially pronounced when the laminations are of poor quality. Reproducibility between counters is controlled both by the quality and clarity of the varves, and of the experience and expertise of the observers. As expected for the sediments in this study, that included multiple intervals of indistinct and low-quality varves, ~~Our results indicate that despite the observers having had minimal experience identifying varves and the poor quality of the sediment, t~~the percentage difference between observers for the total varve years for the same core was ~~only somewhat~~ higher than values reported in the literature. Our varve-only results indicate a range of 14.5-23.6% difference for the same core, compared to 0.8-7.5% reported in (Fortin et al., 2019) or 2.2% in (Tian et al., 2005). Although lamination clarity is most likely the primary source of the range between counters, ~~It is~~the relative lack of experience of the observers may have also contributed to this result ~~not known whether expertise level or sediment quality played a bigger role in increasing the differences.~~. Regardless of the source of the uncertainty, the methodology presented here greatly reduces the disagreement between observers ~~In consideration of the subjective element of observer judgement, the integrated approach attempts to put less emphasis on the observers and tends to align discrepancies.~~ , as ~~T~~the integrated model has ~~shrinks the~~ differences ~~down to~~of 2.6-7.3%, representing a increase in agreement by a factor of three to five.~~.~~ We consider this a significant advantage of this approach, as it objectively the subjective element of observer judgement, puts less emphasis on the observers and tends to align discrepancies.

Formatted: Not Highlight
Formatted: Not Highlight
Formatted: Not Highlight
Formatted: Not Highlight
Formatted: Not Highlight
Formatted: Not Highlight
Formatted: English (United Kingdom)

5.1.~~3~~4 Technical errors

Technical errors in Columbine Lake varve chronology are likely limited to the sediment embedding and thin-sectioning process rather than the coring stage. All cores were remarkably similar (Appendix A Fig. A1), and layers could easily be correlated macroscopically suggesting the coring process did not disturb the sediment. Although thin sections were overlapped to minimize sediment loss, the microscopic analysis revealed cross-sectional splits, or ~~-~~gaps, ~~across the sediment~~ in the middle of thin sections likely due to the embedding process. While infrequent, we accounted by using varve code 6 for the uncertainty associated with the potential that the distorted sediment at the edges of these gaps would impede accurate lamination delineation ~~by using varve code 6, which tried to quantify the missing sediment~~. Varve code 6 added an average of 1.2 and 1.7 cm to COL17-3 and COL17-2, respectively. Furthermore ~~varveRTh~~the varve-only models ~~provides a means of estimating~~ quantify this uncertainty.

5.1.~~3~~5 Rapid depositional events

Errors associated with rapid depositional events were also likely limited to the topmost part of the record. Two thick layers were found in COL17-2 (1.2-2 and 8.5-9.7 cm) and one in COL17-3 (1.5-2.5 cm). The oldest of the two layers in COL17-2 corresponds to a section of indistinct laminations in COL17-3 (7-8 cm). In situations where one core contains rapid depositional events, but the other does not, ~~varveR~~the varve-only models ~~attempts~~attempt to correct for the missing varves by using information from both cores. In the case of the oldest layer in COL17-2, only partial information was available from the other core (COL17-3) because of the indistinct laminations. As a result, information was filled in by the varve emulator which assumed that varves should be present at that depth. This assumption is likely valid in this case but highlights the emulator ~~should~~ must be used along with a detailed understanding of the stratigraphy. ~~with caution.~~

~~5.2 Varve formation mechanism~~

~~Clastic varves generally form in lakes with (1) favorable catchment properties, lake bathymetry, and hydrology, (2) an absence of sediment mixing, and (3) a seasonally variable and significant flux of different components (Anderson et al., 1985; Ojala et al., 2012; Zolitschka et al., 2015). Due to its remarkably clear water and popularity as a backcountry hiking destination, we could not obtain permitting to instrument Columbine lake to monitor sediment deposition. Therefore, our understanding of its non-glacial clastic varve formation mechanism is based on field observations, satellite imagery, and proxy data. Weather data from the region also inform this understanding.~~

~~Non-glacial clastic varves form in catchments containing fine-grained silt and clay material, where at least one inflow is present, and where the bathymetry is deep compared to the surface area (Ojala et al., 2000; Zolitschka et al., 2015). In Columbine Lake, most of the catchment (96%) is unvegetated (Arcusa et al., 2019). The production of siliciclastic fine-grained material is likely dominated by the freeze-thaw cycle and hydrolysis. The eroded material is then entrained into the lake from~~

the margins and via an inflow located to the northwest (Fig. 1). An older inflow is visible from satellite imagery just south of the modern inflow that may also activate during wetter periods. Upon entering the lake, coarser grains settle out first as the energy dissipates and the finer material reaches the coring site. The relatively deep pocket (27 m) where the coring site is located fits the description of a plain sediment depression (Ojala et al., 2000), where depth allows for anoxic conditions and continuous sedimentation and width prevents slope slumping and episodic turbidity currents (O'Sullivan, 1983).

The absence of sediment mixing, crucial for varve formation, generally relates to conditions that deter bioturbation (Anderson et al., 1985; Zolitschka et al., 2015). Perennial anoxia, or meromixis, or situations where oxygenation is infrequent enough to deter organism establishment are typical conditions. The deep plain depression where the coring sites are located likely contributed to this condition, although instrumental data of the water column is unavailable to check for anoxia. Moreover, acidic lake water (pH 5) may be an additional deterrent to benthic biota.

The seasonal sediment transfer in an alpine non-glaciated catchment is usually related to the annual freeze-thaw cycle and runoff events (e.g. snowmelt and rainfall) (Zolitschka et al., 2015). Three types of clastic varves are found in Columbine Lake with distinct structure, and understanding their formation requires separate mechanisms. Clastic varves are typically composed of a coarse-grained lower and a fine-grained upper lamina produced by a nival discharge followed by winter settling (Zolitschka et al., 2015). Such a progression is found in Columbine Lake's type 1 varves, but not type 2 nor 3. Like previous studies (Cuven et al., 2010), we interpret the type 1 varves silt base (lithozone I) as deposition during the snowmelt season and the clay top (lithozone II) to the settling of fines under ice cover. Two mechanisms can produce the structure of lithozone I. One possibility is that in the first weeks of snowmelt, the frozen ground and riverbanks inhibit sediment transportation. The resulting stream with low sediment concentration produces overflow conditions. Once in the distal basin, the sediment settles rapidly in ungraded or fining upward sequences (Francus et al., 2008). Alternatively, the initial melt release may occur before the stratification of the lake (Palmer et al., 2019). Either way, we interpret type 1 lithozone I as low-energy, low sediment concentration, nival discharge. The gradual contact between the lithozone I and II may indicate a slow shut down of turbulence by a slow freeze over and a prolonged period of settling (Desloges, 1994). The sharp contact between lithozone II and the following lithozone I possibly represents the erosive waxing head of the flow, even if the flow is low-energy (Mulder et al., 2001).

In contrast, type 2 varves are composed of subparts that do not follow the typical silt-to-clay progression. The transition from lithozone I interpreted as low energy nival discharge to lithozone II that is interpreted as winter settling is often interrupted by lithozone III, a coarse sub-lamina. The combination of lithozone I and III gives the impression of a single sub-laminae with reverse grading. However, because an erosive contact is sometimes evident between lithozone I and III, this interpretation is likely ruled out. Instead, a second possible explanation is a high-energy event occurring during or after snow melt but before freezing over. The San Juan Mountains experience a bimodal precipitation regime with abundant snow in the winter followed

by violent summer thunderstorms. These short-lived summer events may have the energy to transport coarser material than during the nival snowmelt. As identified in other settings (Cuven et al., 2010), we interpret lithozone III as discharge events produced by high-intensity rainfall occurring during or after the spring melt.

In varve type 3, lithozone I is replaced with lithozone IV. Rather than a coarse event interruption like lithozone III, lithozone IV is composed of a single lamina with an inversely graded transition from a dark and fine bottom to light and coarse top (Fig. 4c). Inversely graded sediment has only rarely been described in lake sediment (Desloges, 1994; Francus et al., 2008; Guyard et al., 2007; Lewis et al., 2010; Palmer et al., 2019). The primary suggested deposition mechanism is the increasing underflow velocity of a hyperpycnal flow during the initiation of a flood (Gilli et al., 2013; Lamb and Mohrig, 2009; Mulder et al., 2001). This depletive (slower velocity with distance) waxing (increasing velocity with time) flow generated by the steadily increasing discharge (rising limb) at a river mouth (Kneller, 1995) has been attributed to secondary pulses of sediment in the summer (Desloges, 1994), variable flow from precipitation events (Lewis et al., 2010), and lateral flow of the sediment to the core site (Palmer et al., 2019). Although possible, this mechanism would require specific discharge rates and sediment concentrations to produce a current that increases in velocity to a critical discharge rate and is denser than the lake water in which it enters (Mulder and Syvitski, 1995).

An alternative hypothesis to explain the inversely graded sediment is specific to Columbine Lake and builds on the evidence of dust-sized sediment in the coarse top of lithozone IV (particle size 5-25 µm). A previous study of Columbine Lake demonstrated that mineral dust transported from the Southwestern deserts make up 30-57% of the sediment (Arcusa et al., 2019). As the mode grain size of the dust (22 µm; Neff et al., 2008; Routson et al., 2016) falls within the grain size range of the top of lithozone IV (Fig. 4c) and dust is regularly found settled on snow in the catchment and on the frozen lake surface (Appendix A Fig. A11), it is conceivable that the coarse top of lithozone IV would be composed of dust brought into the lake in one or a combination of three ways. First, dust can accumulate on the lake ice cover and be released as the ice melts, and this may be later than the onset of snowmelt from the catchment that would create type 1 varves. Second, as snow melts around the dust particles deposited in the catchment, the concentration of the dust left behind increases (Conway et al., 1996; Li et al., 2013). A precipitation event late in the nival season could eventually wash the dust into the lake creating the appearance of inverse grading. Third, the dust-sized material is not dust but catchment material the size of dust brought in from lake margins or the inlet late or at the peak of the nival season. Varve formation due to aeolian dust has been documented previously (Zhai et al., 2006), but whether the inversely graded subparts are due to additions of dust and/or hyperpycnites is unclear from the evidence currently available.

5.3 Varve formation through the Late Holocene

Three transitions in the varve formation are evident from the stratigraphy and varve analysis. These transitions are either abrupt or gradual and likely reflect important changes in the catchment conditions and/or climate. These transitions will be discussed

in turn, from oldest to youngest. Ages and their highest probability density regions (2.5-97.5 %) are indicated from the integrated chronology.

The most abrupt transition in the sequence occurs around 1120 (HDR: 1358-736) BCE (3137, 2753-3375 BP) with the onset of varve formation (Fig. 4) at the contact between units 5 and 4. The processes that can create and sustain conditions necessary for varve formation relate to the physical and chemical properties of the lake water that produce anoxic conditions. These factors include temperature, wind exposure, increased production, and decreased lithogenic influx (Boehrer et al., 2017; Butz et al., 2017; Makri et al., 2020). In the case of Columbine Lake, lithogenic elements (Ti, Ba, Rb, K) decrease, and Mn/Fe temporarily increases at the transition and is low thereafter (Appendix A Figures A4 and A5). When uncorrelated with detrital elements, as is the case here, high Mn/Fe has been interpreted as high dissolved oxygen concentration in the water column (Naeher et al., 2013). The cause for this momentary increase in oxic conditions is unclear but marks the beginning of the varve formation. Unit 4 directly follows this transition and redox conditions are consistently indicated by the PCA analysis (Fig. 5b).

The second most evident transition occurs around 60-50 cm depth in COL17-3 (as deep as 72 cm in COL17-2) corresponding to 419-882 C.E. in the integrated varve chronology model with the gradual shift from varve type 1 (unit 3) to 2 (unit 2) (Fig. 4 and Fig. 5). Whereas the asynchronicity of the transition in the cores suggests site specific causes (e.g. processes that oppose varve formation), the fact that both cores eventually transition indicates a catchment wide influence. The main distinction of varve type 2 is the presence of sub-laminae that are interpreted as higher-energy rainfall events. The position of these laminae within the lamination set suggests the precipitation event occurred late in the nival season, in summer, or in the fall but before the winter settling commenced. The timing of the transition corresponds broadly with the Dark Ages Cold Period (Helama et al., 2017) generally characterized by increased moisture in the southern Rocky Mountains (Rodysill et al., 2018; Routson et al., 2011) although a period of drought is recorded between 600-700 C.E. at Summitville, 110 km to the south east (Routson et al., 2011). Due to the asynchronicity the timing of the transition cannot be ascertained, and the climatic cause should be interpreted with caution.

The final transition occurs at a depth of 7 cm corresponding to an age of 1874 (1844-1902) C.E. The difference between unit 2 and 1 in the PCA analysis is striking (Fig. 5), with lithogenic inputs distinguishing unit 1 from unit 2. The transition from unit 2 to 1 appears to occur after the deposition of the deepest massive layer (also a section of indistinct varves in COL17-3). As discussed in section 3.2.2, a large proportion of the sediment appears to be dust-sized sediment (Arcusa et al., 2019). Additionally, the last 150 years coincide with a 1.7-fold increase in dust deposition compared to pre-industrial times in the San Juan Mountains (Routson et al., 2019), with two peaks in deposition occurring around 1880 C.E. and 1950 C.E. as seen from previous work at Columbine Lake (Arcusa et al., 2019) as well as other lakes in the region (Neff et al., 2008; Routson et al., 2019, 2016). These peaks correspond to the timing of the massive layers: 1973 (1959-1987) C.E. and 1851 (1824-1876) C.E.

~~It is thus conceivable that the additional dust may have disrupted the varve formation process in the massive layer and may have altered the varve formation mechanism subsequently.~~

~~A final hypothesis for the transition to varve type 3 relates to an increasing, even if slight, human impact on the catchment as indicated by two structures and other evidence of grazing and mining activity (Fig. 5). Although the catchment is not accessible by road, a rock shelter was constructed on the south shore. The high alpine meadows have been subject to sheep and cattle grazing since the late middle to late 1800s (Baker, 2020) coinciding with the increased lake productivity indicators seen in unit 1 (Fig. 5). The increased productivity and organic content could explain the thicker varves but not the reverse grading. Secondly, a 2-m-high dam was constructed at the outlet for Mill Creek presumably sometime around the turn of the 20th century, to raise the lake water level and secure water rights for a downstream mine (pers. comm., Forest Service at San Juan National Forest). This water level increase and fluctuation could have increased erosion and reworking of hillslope sediment. Finally, mining became increasingly prevalent in the area from the 1800s (Blair and Bracksieck, 2011), although we did not find evidence for mining within the catchment. Mining indicators (e.g. Guyard et al., 2007) such as silver and zinc become abundant in unit 1, and the increase in heavy metals could have changed both lake productivity and signal a change in lithogenic input. Whether the unique varve type 3 reflects the input of dust or sediment from shoreline or hillslope sources, or changes in lake productivity, or all these factors together, the change occurs in the industrial period and is likely related to human activities within and beyond the catchment.~~

5.~~4~~ 2 Integrating varves with radiometry

Radiometric (^{14}C, ^{210}Pb, ^{137}Cs) profiles are frequently used to validate varve chronologies (Ojala et al., 2012; Zolitschka et al., 2015); however, ages derived from radiometric profiles are generally systematically older than the varve chronology for various reasons (Bonk et al., 2015; Tian et al., 2005; Żarczyński et al., 2018). As the ~~varveR~~ varve-only ~~output~~ model for Columbine Lake consistently shows this divergence (Fig. ~~8~~f7f) we now discuss the merits and pitfalls of integrating the varve chronology with the independent radiometric age-depth model by exploring three possibilities: (1) the ~~varveR~~varve-only model is accurate and the calibrated ^{14}C dates are older than the true sediment ages; (2) the calibrated ^{14}C dates are accurate and the ~~varveR~~varve-only model underestimates the true sediment ages; or (3) both the model and the calibrated ^{14}C dates have unknown systematic biases.

Radiocarbon dating in high-elevation lake sediments is often challenged by a paucity of adequate organic material (~~e.g.~~e.g., Arcusa et al., 2020; Schneider et al., 2018). To gather enough material for a standard ~~graphite-based~~graphite based AMS measurement, the radiocarbon samples in this study were composed of a mixture of aquatic and terrestrial material (Table 3). Samples of mixed composition have been shown to yield ages that are generally too old (Zander et al., 2019). Both aquatic and terrestrial macrofossils are associated with processes that can increase their apparent age. For example, aquatic organisms are subject to a hardwater effect due to dissolved inorganic carbon synthetization (Geyh et al., 1998, 1999), whereas terrestrial

material might be significantly older than the enclosing sediment because of the lags between growth and deposition (Bonk et al., 2015). At least one of the seven radiocarbon dates is likely too old (IonPlus 3527), exceeding Bacon's 95 % uncertainty band (Fig. ~~8f~~7f). A leave-one-out cross-validation analysis (~~e.g.~~e.g., Parnell et al., 2011) could help identify other outliers but the analysis was not undertaken in this study. Despite the potential for other samples being too old, the integrated chronology overlaps with all other radiocarbon samples (Fig. ~~9b~~8b), and the divergence between symmetrical ~~varveR~~varve-only and the radiometric independent model appear to increase with depth (Fig. ~~8f~~7f), both of which support the accuracy of the varve-based age model.

A younger varve chronology compared to the independent model would indicate varve under-counting. Varve count underestimation is recognized in sediment with poor varve appearance (Tian et al., 2005) and depending on the method used in building the chronology (Żarczyński et al., 2018). As discussed in section 5.1, both the sediment microstructures and the quality of the varve appearance are important sources of uncertainty in Columbine Lake: varves are thin, complex, and their formation mechanism appears to change through time. Additionally, the varve emulator is unlikely to have over-estimated the varve counts given the relatively stable sedimentation rate through time. Although observer bias does not appear important, since age deviations from the mean are both positive and negative, and for the reasons listed above, it is most likely that systematic under-counting is prevalent. The integrated model satisfies all available evidence and is more accurate than relying on a single chronological method.

6 Conclusion

We developed a methodology to produce ~~A~~a multi-core, multi-observer integrated radiometric–varve chronology, and demonstrated its utility on a sediment sequence with ~~extending 3137 (−13/+7 %) years was produced from~~ thin, ~~and~~ complex, and intermittent varves from ~~high-elevation~~ Columbine Lake, Colorado. This approach ~~A varve formation model was proposed and was demonstrated to shift through time most likely due to climate in pre-industrial times and human influence within the catchment and on regional dust emissions in industrial times. A Bayesian model was used t~~uses Bayesian learning to integrate these independent sources of age control while quantifying the uncertainties~~y~~ associated with the quality of the varve appearance, the indistinct and intermittent varves, technical issues, observer judgement and depositional events. ~~The varve chronology was integrated with an independent radiometric (^{14}C, ^{210}Pb, and ^{137}Cs) age-depth model to estimate the probabilities of over- and under-counting for different varve quality codes, reduce cumulative uncertainty, and correct for systematic under-counting.~~

This approach for ~~to building a varve~~ chronology development goes beyond the estimation of age uncertainty as it also constrains the uncertainty around varve thickness and thus sedimentation rates. The integration produced estimates of sedimentation rate that combine short-term information ~~(~~primarily informed by lamination thicknesses~~)~~ as well as some long-

term information, ~~native~~ embedded in ~~to~~ both the ~~varve~~ lamination observations and the radiometric ~~chronologies~~data. Furthermore, the approach offers an ensemble of plausible sedimentation rates from which flux and its uncertainty can be calculated. Both the conceptual model presented here, and the codebase itself, has significant potential for extension to other applications that combine layer counting and independent age control estimates, including, for example, layer-counting that relies on geochemical data, single-core or multi-site studies, or ice core or coral chronologies.~~This work not only establishes the chronology and sedimentation rates of Columbine Lake sediment to anchor future research at the site, it also demonstrates the potential for expanding high resolution reconstructions even to sites with indistinct and intermittent varves.~~

7 Appendix A

Table A1. Difference in the number of laminations ~~counts~~ between marker layers between cores for each observer. Note that marker layers do not cross-coordinate between observers, only between cores for each observer. Difference is calculated as COL172 minus ~~-~~COL17-3. For example, marker layer 1 for observer 1 was found at lamination 699 in COL17-2 and at lamination 660 in COL17-3, indicating a difference of 39 laminations. Observers used different marker layers each.

Marker Layer	COL172 (number of laminations)	COL173 (number of laminations)	Difference (COL172-COL173)	Difference (%)
Observer 1				
1	699	660	39	5.7
2	275	308	-33	-11.3
3	951	1230	-279	-25.6
4	439	321	118	31.1
Observer 2				
5	9	8	1	11.8
6	124	74	50	50.5
7	214	187	27	13.5
8	41	91	-50	-75.8
9	203	165	38	20.7
10	442	411	31	7.3
11	180	271	-91	-40.4
12	69	182	-113	-90
13	206	221	-15	-7
14	252	192	60	27
15	128	145	-17	-12.5
Observer 3				
16	9	7	2	25
17	34	25	9	30.5
18	46	30	16	42.1
19	56	21	35	90.9
20	212	177	35	18
21	43	99	-56	-78.9
22	185	169	16	9
23	240	256	-16	-6.5

Formatted Table

24	148	115	33	25.1
25	59	70	-11	-17.1
26	183	266	-83	-37
27	70	242	-172	-110.3
28	80	156	-76	-64.4
29	106	155	-49	-37.5
30	212	193	19	9.4
31	176	139	37	23.5

Formatted: Centered

Marker Layer	COL172	COL173	Observer	Difference (years)	Difference (%)
1	699	660	1	39	5.7
2	275	308	1	-33	-11.3
3	951	1230	1	-279	-25.6
4	439	321	1	118	31.1
5	9	8	2	1	11.8
6	124	74	2	50	50.5
7	214	187	2	27	13.5
8	41	91	2	-50	-75.8
9	203	165	2	38	20.7
10	442	411	2	31	7.3
11	180	271	2	-91	-40.4
12	69	182	2	-113	-90.0
13	206	221	2	-15	-7.0
14	252	192	2	60	27.0
15	128	145	2	-17	-12.5
16	9	7	3	2	25.0
17	34	25	3	9	30.5
18	46	30	3	16	42.1
19	56	21	3	35	90.9
20	212	177	3	35	18.0
21	43	99	3	-56	-78.9
22	185	169	3	16	9.0
23	240	256	3	-16	-6.5
24	148	115	3	33	25.1
25	59	70	3	-11	-17.1
26	183	266	3	-83	-37.0
27	70	242	3	-172	-110.3
28	80	156	3	-76	-64.4
29	106	155	3	-49	-37.5
30	212	193	3	19	9.4
31	176	139	3	37	23.5

Table A2. Observer- and core-specific ~~varve sequence~~lamination statistics of thickness and counts. ~~Varve~~ Lamination quality codes 4, 5, and 6 are excluded from the analysis except to calculate the cumulative length of indistinct sections. All units are millimetres unless otherwise noted.

Core name	COL17-2			COL17-3		
	Obs 1	Obs 2	Obs 3	Obs 1	Obs 2	Obs 3
Minimum thickness	0.05	0.01	0.07	0.03	0.02	0.1
Maximum thickness	2.32	3.64	2.46	4.94	1.69	6.86
Median thickness	0.39	0.48	0.41	0.44	0.51	0.46
Mean thickness	0.43	0.56	0.48	0.48	0.56	0.51
SD thickness	0.23	0.35	0.26	0.24	0.25	0.37
Total indistinct section length	40	10	108	167	57	112

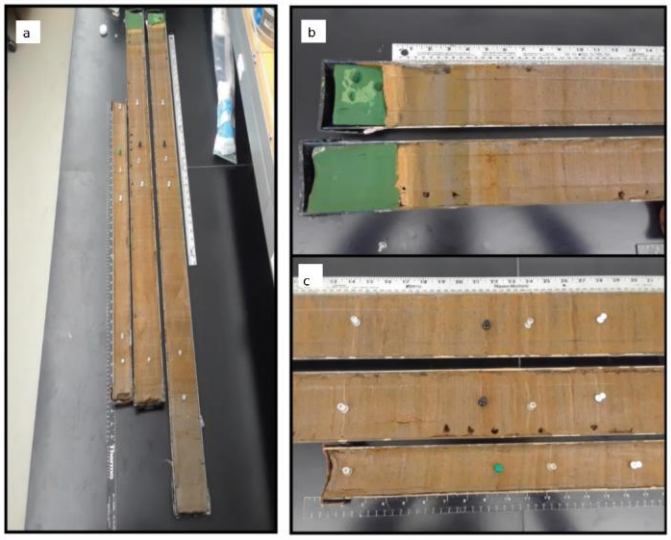

Fig. A1. Tie points from three Columbine Lake cores. (~~A~~a) shows COL-17-2 shown on the far right, COL-17-3 in the middle, and COL-16-1 on the left. The top of cores COL-17-3 and COL-17-2 are shown in (~~B~~b). (~~C~~c) is a section of the middle of all three cores with matching laminations marked with pins. Image credit: Wiman, C. (2019). Late Holocene hydroclimate and productivity in varved sediment at Columbine Lake, Colorado (Master thesis, Northern Arizona University).

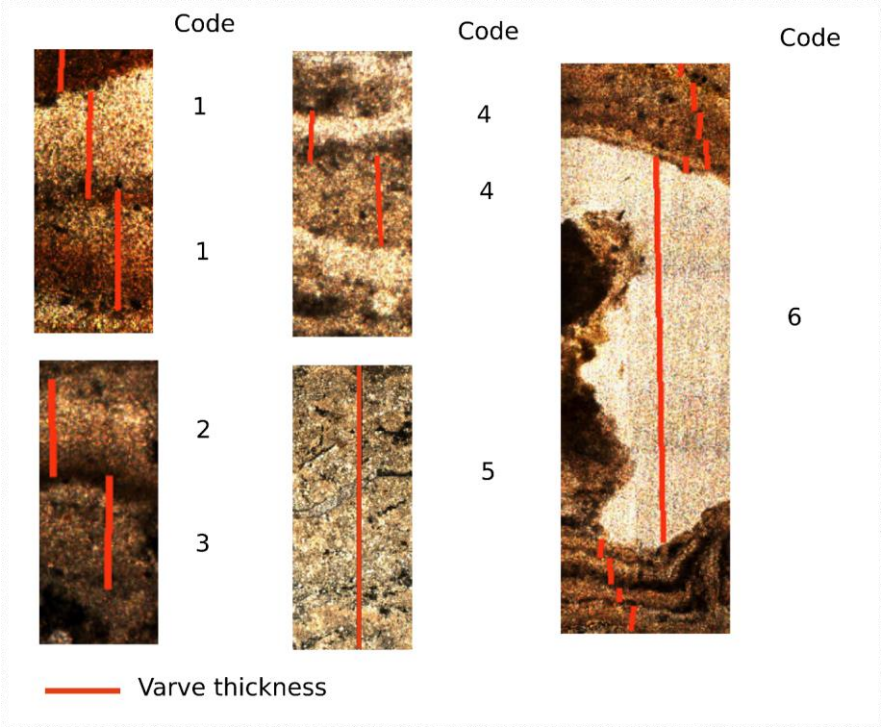

Fig. A2. Examples of varves appearance for each ~~varve~~ lamination quality code. Not to scale. For example only.

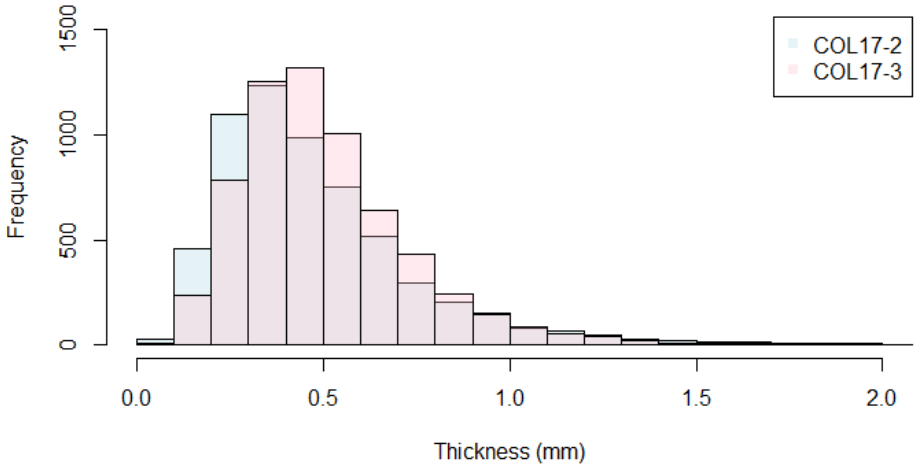

Fig. A3. Comparison of ~~varve~~ lamination thickness measurement~~s~~ from ~~varved~~ sections with (~~codes~~ 1, 2, and 3~~)~~ between COL17-2 and COL17-3. Blue represents COL17-2, red represents COL17-3, while the overlap of the two distributions is light purple.

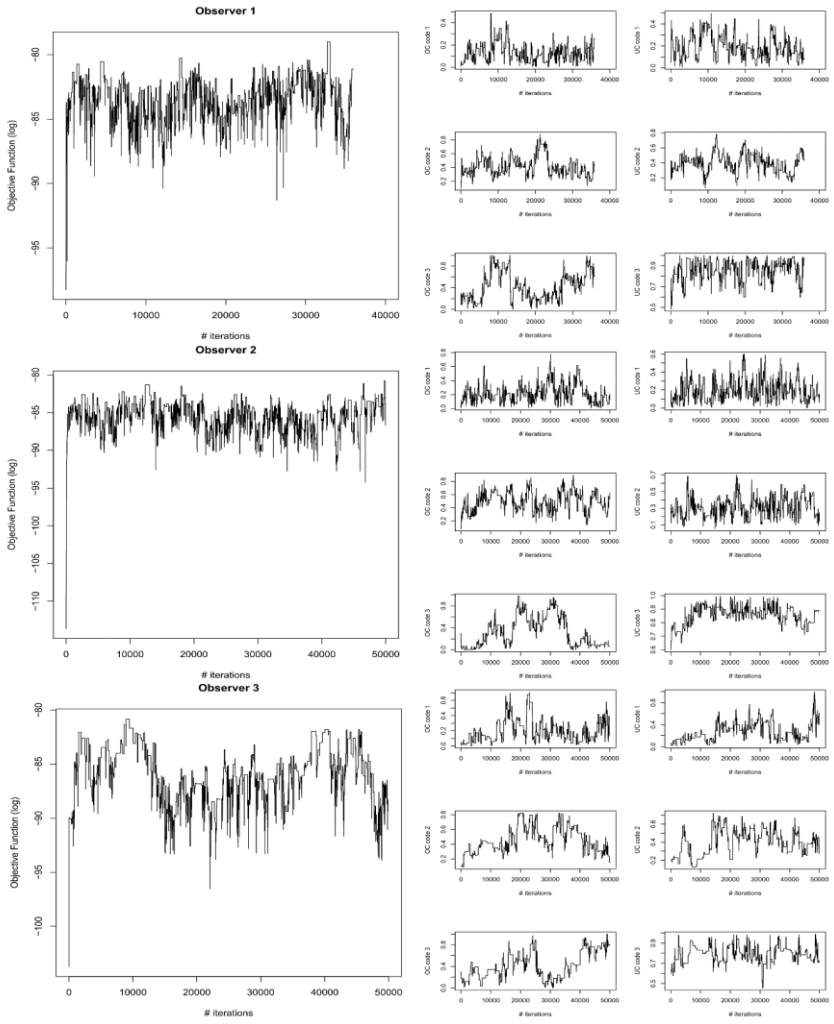

Fig. ~~A8~~A4. Integrated model diagnostics. Objective function output value (left) and counting probabilities (right) for each iteration for observers 1 (top), 2 (middle), 3 (bottom). OC = over-counting. UC = under-counting. Number that follows OC/UC indicates the varve quality code.

830

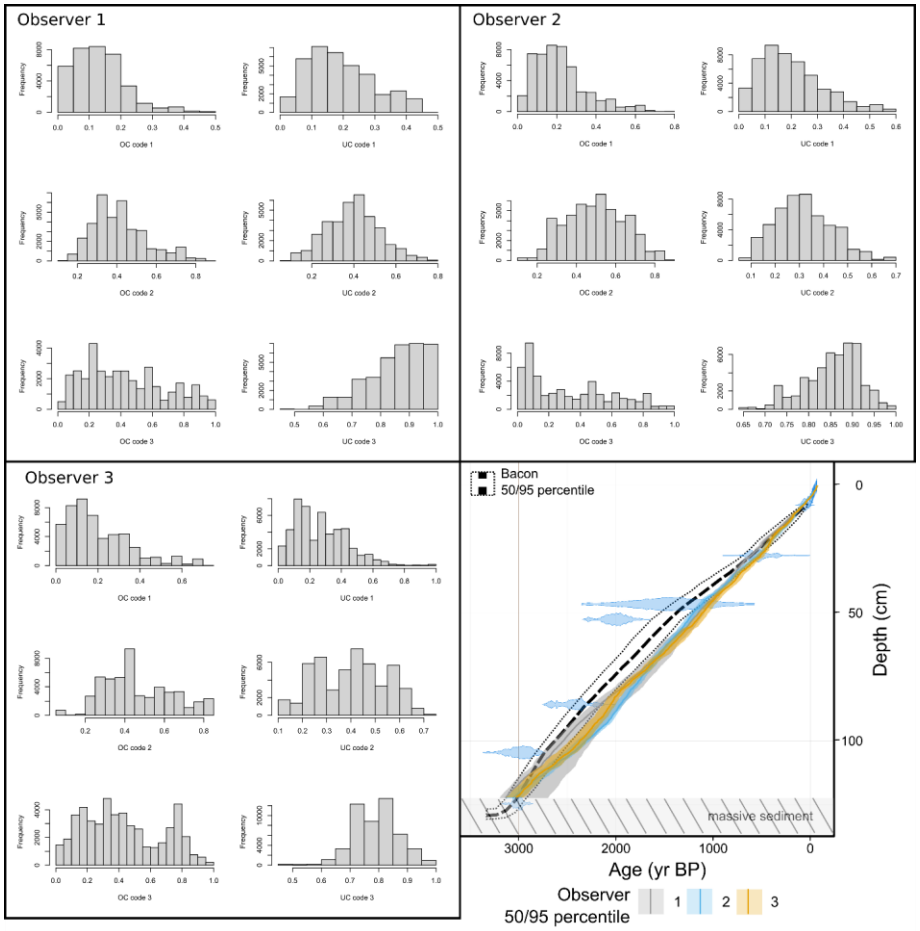

Fig. ~~A9~~A5. Posterior probabilities of over- and under-counting for each observer for core COL17-3. Comparison between independent and integrated age-depth model. OC: over-counting. UC: under-counting. Code 1-3 indicate the ~~varve~~ lamination quality codes 1, 2, 3.

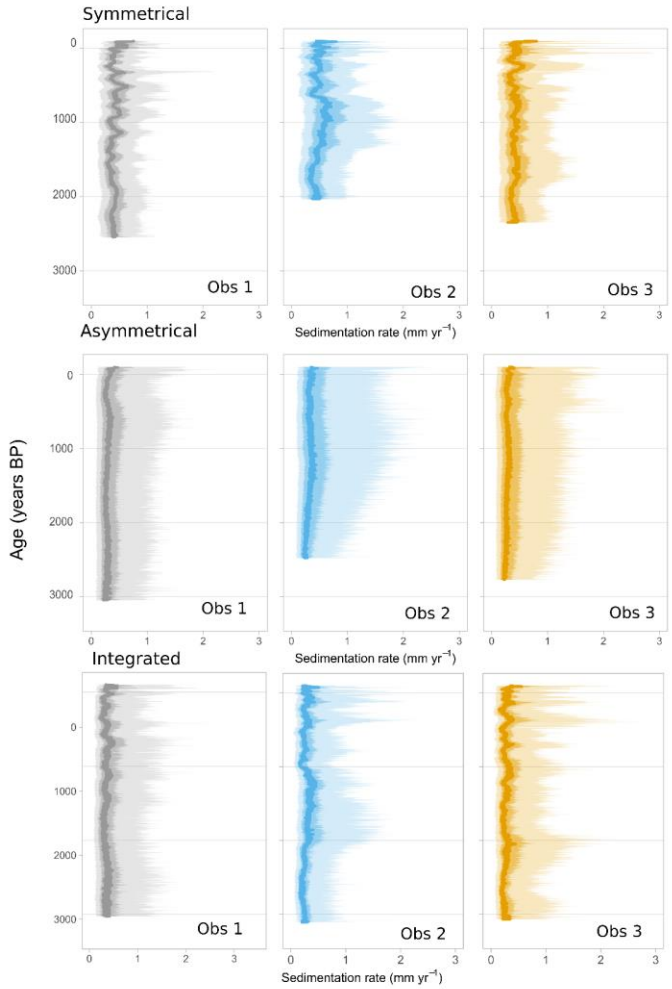

Fig. ~~A10~~A6. Sedimentation rates for each observer for symmetrical ~~varveR~~varve-only model, asymmetrical ~~varveR~~varve-only model and the integrated models.

A) June 2012

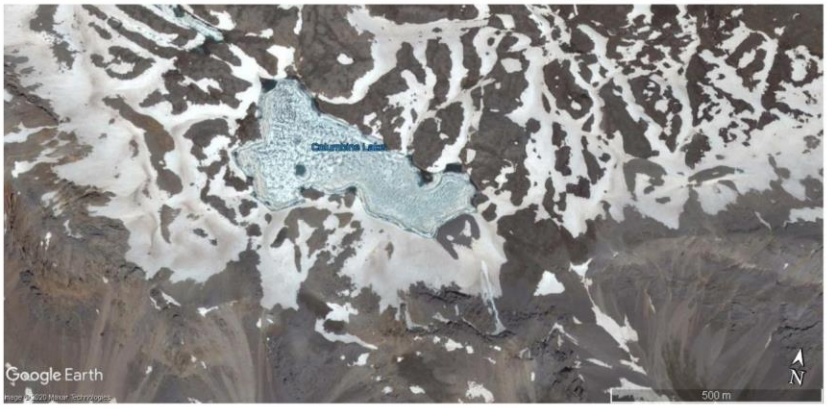

B) June 2014

~~**Fig. A11. Dust deposition in Columbine Lake catchment and frozen surface is frequently visible as a light brown tint on the snow. Image from (a) June 2012, and (b) June 2014. Map data: Google.**~~

8 Code and data availability

Code for the original ~~VarveR~~varveR model can be found at 10.5281/zenodo.4733326. Code for the varve-only and radiometric model integration can be found at 10.5281/zenodo.5771333~~10.5281/zenodo.4744872~~. Datasets containing radiometric measurements from Columbine Lake can be found at ~~https://doi.org/~~10.25384/SAGE.9879209.v1.~~–~~ Datasets of varve delineations can be found at 10.6084/m9.figshare.14251400. Datasets necessary to run the code (LiPD file ~~and,~~ Bacon output file, and serac models) can be found at 10.6084/m9.figshare.14417999 and 10.6084/m9.figshare.17156702.v1. Raw lead and cesium data can be found at https://doi.org/10.6084/m9.figshare.17157245.v1. ~~Dataset containing proxy measurements produced in this study can be found at 10.6084/m9.figshare.14265644 for the review process and will be uploaded to NOAA World Data Service for Paleoclimatology upon publication.~~ Although the developing a full-fledged software package is outside the scope of this study, the authors are interested to work with potential users interested in adapting the codebase for other applications.

Formatted: Default Paragraph Font, English (United Kingdom)

9 Author contribution

SHA and NPM conceptualized the study. CW sampled and embedded the sediments, SHA, CW, and SP measured varves, and SEM measured lead samples. MAL ran the Plum-Bacon model. SHA and NPM created and modified the Bayesian models, and SHA ran the models. SHA visualized the data and drafted the original manuscript. All authors contributed to the review and editing.

10 Competing interests

The authors declare that they have no conflict of interest.

11 Acknowledgments

This research was funded by Bob and Judi Braudy and we are grateful for their support. MAL was partially founded by CONACYT CB-2016-01-284451 and COVID19 312772 grants and a RDCOMM grant. We thank D Buscombe for letting us use the bathymetric equipment, RS Anderson for the identification of macrofossils for ^{14}C dating, K Whitacre for lab assistance, Rosalind Wu from the San Juan National Forest Service for working with us to obtain permits for sampling Columbine Lake, C Routson and D Kaufman for helpful feedback on the manuscript, Quality Thin Sections for producing the thin sections, and C Ebert for conducting ^{14}C dating at IonPlus in Zurich. We thank E Yackulic, C Mogen, W Wiman, C Routson, A Wong, A Platt, J Chaffeur, E Broadman, and M Caron for the help in the field.

12 References

Anderson, B. R. Y., Dean, W. E., Bradbury, P. and Love, D.: Meromictic Lakes and Varved Sediments, 19 [online] Available from: https://pubs.usgs.gov/bul/1607/report.pdf, 1985.

Anderson, R. S., Smith, S. J., Lynch, A. M. and Geils, B. W.: The pollen record of a 20th century spruce beetle (*Dendroctonus rufipennis*) outbreak in a Colorado subalpine forest, USA, For. Ecol. Manage., 260(4), 448–455, doi:10.1016/j.foreco.2010.05.001, 2010.

Appleby, P.: Chronostratigraphic techniques in recent sediments, in Tracking Environmental Change Using Lake Sediments. Volume 1, edited by W. Last and J. P. Smol, pp. 171–203, Kluwer Academic Publishers, Dordrecht., 2001.

Appleby, P. G. and Oldfield, F.: The calculation of lead-210 dates assuming a constant rate of supply of unsupported ^{210}Pb to the sediment, CATENA, 5(1), 1–8, doi:10.1016/S0341-8162(78)80002-2, 1978.

Aquino-López, M. A., Blaauw, M., Christen, J. A. and Sanderson, N. K.: Bayesian Analysis of ^{210}Pb Dating, J. Agric. Biol. Environ. Stat., 23, 317–333, doi:10.1007/s13253-018-0328-7, 2018.

Arcusa, S. H., McKay, N. P., Routson, C. C. and Munoz, S. E.: Dust-drought interactions over the last 15,000 years: A network of lake sediment records from the San Juan Mountains, Colorado, The Holocene, doi:10.1177/0959683619875192, 2019.

Arcusa, S. H., Schneider, T., Mosquera, P. V., Vogel, H., Kaufman, D. S., Szidat, S. and Grosjean, M.: Late Holocene tephrostratigraphy from Cajas National Park, southern Ecuador, Andean Geol., 47(3), 508–528, doi:http://dx.doi.org/10.5027/andgeoV47n3-3301, 2020.

Baker, W. L.: Variable forest structure and fire reconstructed across historical ponderosa pine and mixed conifer landscapes of the San Juan Mountains, Colorado, Land, 9(1), 1–35, doi:10.3390/land9010003, 2020.

Blaauw, M. and Christen, J. A.: Flexible paleoclimate age-depth models using an autoregressive gamma process, Bayesian Anal., 6(3), 457–474, doi:10.1214/11-BA618, 2011.

Blair, R. and Bracksieck, G.: The Eastern San Juan Mountains., edited by R. Blair and G. Bracksieck, University Press of Colorado., 2011.

Blockley, S. P. E., Ramsey, C. B., Lane, C. S. and Lotter, A. F.: Improved age modelling approaches as exemplified by the revised chronology for the Central European varved lake Soppensee, Quat. Sci. Rev., 27(1–2), 61–71, doi:10.1016/j.quascirev.2007.01.018, 2008.

Boers, N., Goswami, B. and Ghil, M.: A complete representation of uncertainties in layer-counted paleoclimatic archives, Clim. Past, 13(9), 1169–1190, doi:10.5194/cp-13-1169-2017, 2017.

Bonk, A., Tylmann, W., Goslar, T., Wacnik, A. and Grosjean, M.: Comparing varve counting and ^{14}C-AMS chronologies in the sediments of lake Żabińskie, Northeastern Poland: Implications for accurate ^{14}C dating of lake sediments, Geochronometria, 42, 159–171, 2015.

Brauer, A., Hajdas, I., Blockley, S. P. E., Bronk Ramsey, C., Christl, M., Ivy-Ochs, S., Moseley, G. E., Nowaczyk, N. N., Rasmussen, S. O., Roberts, H. M., Spötl, C., Staff, R. A. and Svensson, A.: The importance of independent chronology in

integrating records of past climate change for the 60-8ka INTIMATE time interval, Quat. Sci. Rev., 106, 47–66, doi:10.1016/j.quascirev.2014.07.006, 2014.

Bronk Ramsey, C.: Radiocarbon calibration and analysis of stratigraphy: the OxCal program, Radiocarbon, 37(2), 425–430, 1995.

Bruel, R. and Sabatier, P.: serac: a R package for ShortlivEd RAdionuclide Chronology of recent sediment cores, 1–38, doi:10.31223/osf.io/f4yma, 2020.

Buck, C. E., Higham, T. F. G. and Lowe, D. J.: Bayesian tools for tephrochronology, The Holocene, 13(5), 639–647, doi:10.1191/0959683603hl652ft, 2003.

~~Butz, C., Grosjean, M., Poraj-Górska, A., Enters, D., Tylmann, W. and Butz, C.: Sedimentary Bacteriopheophytin a as an indicator of meromixis in varved lake sediments of Lake Jaczno , north-east Poland , AD 1891 – 2010, Glob. Planet. Change, 144, 1–26, doi:10.1016/j.gloplacha.2016.07.012, 2016.~~

~~Butz, C., Grosjean, M., Goslar, T. and Tylmann, W.: Hyperspectral imaging of sedimentary bacterial pigments: a 1700-year history of meromixis from varved Lake Jaczno, northeast Poland, J. Paleolimnol., 58(1), 57–72, doi:10.1007/s10933-017-9955-1, 2017.~~

Carrara, P.: Deglaciation and postglacial treeline fluctuation in the northern San Juan Mountains, Colorado, U.S. Geol. Soc. Prof. Pap. 1782, 1–48 [online] Available from: http://pubs.usgs.gov/pp/1782/, 2011.

~~Conway, H., Gades, A. and Raymond, C. F.: Albedo of dirty snow during conditions of melt, Water Resour. Res., 32(6), 1713–1718, 1996.~~

~~Cuven, S., Francus, P. and Lamoureux, S. F.: Estimation of grain size variability with micro X-ray fluorescence in laminated lacustrine sediments, Cape Bounty, Canadian High Arctic, J. Paleolimnol., 44(3), 803–817, doi:10.1007/s10933-010-9453-1, 2010.~~

~~Dean, W. J.: Determination of carbonate and organic matter in calcareous sediments and sedimentary rocks by loss on ignition: comparison with other methods, J. Sediment. Petrol., 44(I), 242–248, doi:10.1128/JCM.01030-15, 1974.~~

~~Desloges, J. R.: Varve deposition and the sediment yield record at three small lakes of the southern Canadian Cordillera, Arct. Alp. Res., 26(2), 130–140, doi:10.2307/1551776, 1994.~~

Dräger, N., Theuerkauf, M., Szeroczyńska, K., Wulf, S., Tjallingii, R., Plessen, B., Kienel, U. and Brauer, A.: Varve microfacies and varve preservation record of climate change and human impact for the last 6000 years at Lake Tiefer See (NE Germany), The Holocene, 27(3), 450–464, doi:10.1177/0959683616660173, 2017.

Fortin, D., Praet, N., McKay, N. P., Kaufman, D. S., Jensen, B. J. L., Haeussler, P. J., Buchanan, C. and De Batist, M.: New approach to assessing age uncertainties – The 2300-year varve chronology from Eklutna Lake, Alaska (USA), Quat. Sci. Rev., 203, 90–101, doi:10.1016/j.quascirev.2018.10.018, 2019.

~~Francus, P., Bradley, R. S., Lewis, T., Abbott, M., Retelle, M. and Stoner, J. S.: Limnological and sedimentary processes at Sawtooth Lake, Canadian High Arctic, and their influence on varve formation, J. Paleolimnol., 40(3), 963–985, doi:10.1007/s10933-008-9210-x, 2008.~~

Geyh, M., Schotterer, U. and Grosjean, M.: Temporal changes of the ^{14}C reservoir effect in lakes, Radiocarbon, 40(2), 921–931, 1998.

Geyh, M. A., Grosjean, M., Núñez, L. and Schotterer, U.: Radiocarbon reservoir effect and the timing of the late-glacial/early Holocene humid phase in the Atacama Desert (Northern Chile), Quat. Res., 52(2), 143–153, doi:10.1006/qres.1999.2060, 1999.

Gilli, A., Anselmetti, F. S., Glur, L. and Wirth, S. B.: Lake Sediments as Archives of Recurrence Rates and Intensities of Past Flood Events, in Dating Torrential Processes on Fans and Cones, edited by M. Schneuwly-Bollschweiler, pp. 225–242, Springer Science+Business Media, Dordrecht., 2013.

Guyard, H., Chapron, E., St-Onge, G., Anselmetti, F. S., Arnaud, F., Magand, O., Francus, P. and Res, M. A.: High-altitude varve records of abrupt environmental changes and mining activity over the last 4000 years in the Western French Alps (Lake Bramant, Grandes Rousses Massif), Quat. Sci. Rev., 26, 2644–2660, doi:10.1016/j.quascirev.2007.07.007, 2007.

Helama, S., Jones, P. D. and Briffa, K. R.: Dark Ages Cold Period: A literature review and directions for future research, Holocene, 27(10), 1600–1606, doi:10.1177/0959683617693898, 2017.

Hughen, K. A., Southon, J. R., Bertrand, C. J. H., Frantz, B. and Zermeño, P.: Cariaco basin calibration update: Revisions to calendar and ^{14}C chronologies for core PL07-58PC, Radiocarbon, 46(3), 1161–1187, doi:10.1017/S0033822200033075, 2004.

Juggins, S.: rioja: Analysis of Quaternary Science Data, [online] Available from: https://cran.r-project.org/package=rioja, 2020.

Kneller, B.: Beyond the turbidite paradigm: Physical models for deposition of turbidites and their implications for reservoir prediction, Geol. Soc. Spec. Publ., 94(December), 31–49, doi:10.1144/GSL.SP.1995.094.01.04, 1995.

Krishnaswamy, S., Lal, D., Martin, J. M. and Meybeck, M.: Geochronology of lake sediments, Earth Planet. Sci. Lett., 11(1–5), 407–414, doi:10.1016/0012-821X(71)90202-0, 1971.

Lamb, M. P. and Mohrig, D.: Do hyperpycnal-flow deposits record river-flood dynamics? Geology, 37(12), 1067–1070, doi:10.1130/G30286A.1, 2009.

Lamoureux, S. F.: Embedding unfrozen lake sediments for thin section preparation, J. Paleolimnol., 10(2), 141–146, 1994.

Lamoureux, S.F.. Varve chronology techniques. In: Last, W.M., Smol, J.P. (Eds.), Developments in Paleoenvironmental Research (DPER), Tracking Environ- mental Change Using Lake Sediments: Basin Analysis, Coring, and Chronological Techniques, vol. 1. Kluwer, Dordrecht, pp. 247e260. http://dx.doi.org/10. 1007/0-306-47669-X_11, 2001.

Le, S., Josse, J. and Husson, F.: FactoMineR: An R package for multivariate analysis, J. Stat. Softw., 25(1), 1–18, 2008.

Lewis, T., Francus, P., Bradley, R. S. and Kanamaru, K.: An automated system for the statistical analysis of sediment texture and structure at the micro scale, Comput. Geosci., 36(10), 1374–1383, doi:10.1016/j.cageo.2010.03.018, 2010.

Li, J., Okin, G. S., McKenzie Skiles, S. and Painter, T. H.: Relating variation of dust on snow to bare soil dynamics in the western United States, Environ. Res. Lett., 8(4), doi:10.1088/1748-9326/8/4/044054, 2013.Lima, A.L., Hubeny, J.B., Reddy, C.M., King, J.W., Hughen, K.A. and Eglinton, T.I.: High-resolution historical records from Pettaquamscutt River basin

Formatted: English (United States)

sediments: 1. 210Pb and varve chronologies validate record of 137Cs released by the Chernobyl accident. Geochimica et Cosmochimica Acta 69.7 (2005): 1803-1812, 2005.

Lipman, P. W. and Mcintosh, W. C.: Tertiary Volcanism in the Eastern San Juan Mountains, in The Eastern San Juan Mountains: Their Geology, Ecology, Human History, edited by R. Blair and G. Bracksieck, University Press of Colorado., 2011.

Makri, S., Rey, F., Gobet, E., Gilli, A., Tinner, W. and Grosjean, M.: Early human impact in a 15,000-year high-resolution hyperspectral imaging record of paleoproduction and anoxia from a varved lake in Switzerland, Quat. Sci. Rev., 239, 106335, doi:10.1016/j.quascirev.2020.106335, 2020.

McKkay, N., Emile-Geay, J. and Khider, D.: gGeoChronR – an R package to model, analyze, and visualize age-uncertain data, Geochronology, 3, 149-169, https://doi.org/10.5194/gchron-3-149-2021, 2021.

McKay, N. P.: Development package for varve counting, modeling and analysis., 2019.

Mortlock, R. A. and Froelich, P. N.: A simple method for the rapid determination of biogenic opal in pelagic marine sediments, Deep Sea Res. Part A, Oceanogr. Res. Pap., 36(9), 1415–1426, doi:10.1016/0198-0149(89)90092-7, 1989.

Mulder, T. and Syvitski, J. P. M.: Turbidity currents generated at river mouths during exceptional discharges to the world oceans, J. Geol., 103(3), 285–299, doi:10.1086/629747, 1995.

Mulder, T., Migeon, S., Savoye, B. and Faugeres, J. C.: Inversely graded turbidite sequences in the deep Mediterranean: A record of deposits from flood-generated turbidity currents? Geo-Marine Lett., 21(2), 86–93, doi:10.1007/s003670100071, 2001.Munoz, S.E., Giosan, L., Blusztajn, J., Rankin, C., Stinchcomb, G.E. Radiogenic fingerprinting reveals anthropogenic and buffering controls on sediment dynamics of the Mississippi River system. Geology, 47 (3), 271–274, https://doi.org/10.1130/G45194.1, 2019.

Nacher, S., Gilli, A., North, R. P., Hamann, Y. and Schubert, C. J.: Tracing bottom water oxygenation with sedimentary Mn/Fe ratios in Lake Zurich, Switzerland, Chem. Geol., 352, 125–133, doi:10.1016/j.chemgeo.2013.06.006, 2013.

Neff, J. C., Ballantyne, A. P., Farmer, G. L., Mahowald, N. M., Conroy, J. L., Landry, C. C., Overpeck, J. T., Painter, T. H., Lawrence, C. R. and Reynolds, R. L.: Increasing eolian dust deposition in the western United States linked to human activity, Nat. Geosci., 1(3), 189–195, doi:10.1038/ngeo133, 2008.

O'Sullivan, P. E.: Annually-laminated lake sediments and the study of Quaternary environmental changes - a review, Quat. Sci. Rev., 1(4), 245–313, doi:10.1016/0277-3791(83)90008-2, 1983.

Ojala, A. E. K. and Tiljander, M.: Testing the fidelity of sediment chronology: Comparison of varve and paleomagnetic results from Holocene lakeHolocene Lake sediments from central Finland, Quat. Sci. Rev., 22(15–17), 1787–1803, doi:10.1016/S0277-3791(03)00140-9, 2003.

Ojala, A. E. K., Saarinen, T. and Salonen, V. P.: Preconditions for the formation of annually laminated lake sediments in southern and central Finland, Boreal Environ. Res., 5(3), 243–255, 2000.

Ojala, A. E. K., Francus, P., Zolitschka, B., Besonen, M. and Lamoureux, S. F.: Characteristics of sedimentary varve chronologies - A review, Quat. Sci. Rev., 43, 45–60, doi:10.1016/j.quascirev.2012.04.006, 2012.

Formatted: Default Paragraph Font, English (United Kingdom)

Palmer, A. P., Bendle, J. M., MacLeod, A., Rose, J. and Thorndycraft, V. R.: The micromorphology of glaciolacustrine varve sediments and their use for reconstructing palaeoglaciological and palaeoenvironmental change, Quat. Sci. Rev., 226, 105964, doi:10.1016/j.quascirev.2019.105964, 2019.Omelchenko A., Lockhart W.L., Wilkinson1 P.: Depositional Characteristics of Lake Sediments in Canada as Determined by Pb-210 and Cs-137. In: Omelchenko A., Pivovarov A.A., Swindall W.J. (eds) Modern Tools and Methods of Water Treatment for Improving Living Standards. NATO Science Series (Series IV: Earth and Environmental Series), vol 48. Springer, Dordrecht, 10.1007/1-4020-3116-5_2, 2005.

Parnell, A. C., Buck, C. E. and Doan, T. K.: A review of statistical chronology models for high-resolution, proxy-based Holocene palaeoenvironmental reconstruction, Quat. Sci. Rev., 30(21–22), 2948–2960, doi:10.1016/j.quascirev.2011.07.024, 2011.

Preibisch, S., Saalfeld, S. and Tomancak, P.: Globally optimal stitching of tiled 3D microscopic image acquisitions, Bioinformatics, 25(11), 1463–1465, doi:10.1093/bioinformatics/btp184, 2009.

R Core Team: R: A Language and Environment for Statistical Computing, [online] Available from: https://www.r-project.org/, 2019.

Rein, B. and Sirocko, F.: In-situ reflectance spectroscopy—analysing techniques for high-resolution pigment logging in sediment cores, Int. J. Earth Sci., 91, 950–954, 2002.

Rodysill, J. R., Anderson, L., Cronin, T. M., Jones, M. C., Thompson, R. S., Wahl, D. B., Willard, D. A., Addison, J. A., Alder, J. R., Anderson, K. H., Anderson, L., Barron, J. A., Bernhardt, C. E., Hostetler, S. W., Kehrwald, N. M., Khan, N. S., Richey, J. N., Starratt, S. W., Strickland, L. E., Toomey, M. R., Treat, C. C. and Wingard, G. L.: A North American Hydroclimate Synthesis (NAHS) of the Common Era, Glob. Planet. Change, 162(December 2017), 175–198, doi:10.1016/j.gloplacha.2017.12.025, 2018.

Routson, C. C., Woodhouse, C. A. and Overpeck, J. T.: Second century megadrought in the Rio Grande headwaters, Colorado: How unusual was medieval drought? Geophys. Res. Lett., 38(22), 1–5, doi:10.1029/2011GL050015, 2011.

Routson, C. C., Overpeck, J. T., Woodhouse, C. A. and Kenney, W. F.: Three millennia of southwestern north American dustiness and future implications, PLoS One, 11(2), 1–20, doi:10.1371/journal.pone.0149573, 2016.

Routson, C. C., Arcusa, S. H., McKay, N. P. and Overpeck, J. T.: A 4500-year-long record of southern Rocky Mountain dust deposition, Geophys. Res. Lett., 46, 2019GL083255, doi:10.1029/2019GL083255, 2019.

Schlolaut, G., Marshall, M. H., Brauer, A., Nakagawa, T., Lamb, H. F., Staff, R. A., Bronk Ramsey, C., Bryant, C. L., Brock, F., Kossler, A., Tarasov, P. E., Yokoyama, Y., Tada, R. and Haraguchi, T.: An automated method for varve interpolation and its application to the Late Glacial chronology from Lake Suigetsu, Japan, Quat. Geochronol., 13, 52–69, doi:10.1016/j.quageo.2012.07.005, 2012.

Schneider, T., Hampel, H., Mosquera, P. V., Tylmann, W. and Grosjean, M.: Paleo-ENSO revisited: Ecuadorian Lake Pallcacocha does not reveal a conclusive El Niño signal, Glob. Planet. Change, 168(June), 54–66, doi:10.1016/j.gloplacha.2018.06.004, 2018.

Formatted: Default Paragraph Font, English (United Kingdom)

Sheppard, P. R., Comrie, A. C., Packin, G. D., Angersbach, K. and Hughes, M. K.: The climate of the US Southwest, Clim. Res., 21, 219–238, 2002.

Tian, J., Brown, T. A. and Hu, F. S.: Comparison of varve and ^{14}C chronologies from Steel Lake, Minnesota, USA, The Holocene, 15(4), 510–517, doi:10.1191/0959683605hl828rp, 2005.

Trachsel, M., Grosjean, M., Schnyder, D., Kamenik, C. and Rein, B.: Scanning reflectance spectroscopy (380–730 nm): A novel method for quantitative high-resolution climate reconstructions from minerogenic lake sediments, J. Paleolimnol., 44(4), 979–994, doi:10.1007/s10933-010-9468-7, 2010.

Western Regional Climate Center: Cooperative Climatological Data Summaries, [online] Available from: https://wrcc.dri.edu/cgi-bin/cliMAIN.pl?co7656, 2018.

Yackulic, E.: Productivity and temperature variability over the past 15000 years at a small alpine lake in the southern San Juan Mountains, Colorado, Northern Arizona University., 2017.

Zander, P. D., Szidat, S., Kaufman, D. S., Żarczyński, M., Poraj-górska, A. I. and Grosjean, M.: Miniature radiocarbon measurements (< 150 μg C) from sediments of Lake Żabińskie, Poland: effect of precision and dating density on age-depth models, Geochronology, (December), 63–79, 2019.

Żarczyński, M., Tylmann, W. and Goslar, T.: Multiple varve chronologies for the last 2000 years from the sediments of Lake Żabińskie (northeastern Poland) – Comparison of strategies for varve counting and uncertainty estimations, Quat. Geochronol., 47(January), 107–119, doi:10.1016/j.quageo.2018.06.001, 2018.

Żarczyński, M., Szmańda, J. and Tylmann, W.: Grain-Size Distribution and Structural Characteristics of Varved Sediments from Lake Żabińskie (Northeastern Poland), Quaternary, 2(1), 8, doi:10.3390/quat2010008, 2019a.

Żarczyński, M., Waenik, A. and Tylmann, W.: Tracing lake mixing and oxygenation regime using the Fe/Mn ratio in varved sediments: 2000 year-long record of human-induced changes from Lake Żabińskie (NE Poland), Sci. Total Environ., 657, 585–596, doi:10.1016/j.scitotenv.2018.12.078, 2019b.

Zhai, Q., Guo, Z., Li, Y. and Li, R.: Annually laminated lake sediments and environmental changes in Bashang Plateau, North China, Palaeogeogr. Palaeoclimatol. Palaeoecol., 241(1), 95–102, doi:10.1016/j.palaeo.2006.06.011, 2006.

Zimmerman, S. R. H. and Wahl, D. B.: Holocene paleoclimate change in the western US: The importance of chronology in discerning patterns and drivers, Quat. Sci. Rev., 246, 106487, doi:10.1016/j.quascirev.2020.106487, 2020.

Zolitschka, B., Francus, P., Ojala, A. E. K. and Schimmelmann, A.: Varves in lake sediments - a review, Quat. Sci. Rev., 117, 1–41, doi:10.1016/j.quascirev.2015.03.019, 2015.